

Elisabeth Katharina Schmitt

Continuously Seeded Tubular Crystallizer

Influence of Seed-Loading, Flow Rates and Cooling Trajectory on the
Crystal Size Distribution of APIs and Fine Chemicals

Kontinuierliches Wachstum von Impf- zu Produktkristallen in einem
Rohrkristallisator

DIPLOMA THESIS

(Diplomarbeit zur Erlangung des akademischen Grades einer Diplom-Ingenieurin
der Studienrichtung Technische Chemie/Chemieingenieurwesen an der
Technischen Universität Graz.)

Advisor:

Univ.-Prof. Dipl.-Ing. Dr. techn. Johannes G. Khinast

and

Dipl.-Ing. Rafael Eder

Graz University of Technology

Institute for Process and Particle Engineering
Research Group Pharmaceutical Engineering

Graz, August 2010

Deutsche Fassung:
Beschluss der Curricula-Kommission für Bachelor-, Master- und Diplomstudien vom 10.11.2008
Genehmigung des Senates am 1.12.2008

EIDESSTÄTLICHE ERKLÄRUNG

Ich erkläre an Eides statt, dass ich die vorliegende Arbeit selbstständig verfasst, andere als die angegebenen Quellen/Hilfsmittel nicht benutzt, und die den benutzten Quellen wörtlich und inhaltlich entnommene Stellen als solche kenntlich gemacht habe.

Graz, am

.....
(Unterschrift)

Englische Fassung:

STATUTORY DECLARATION

I declare that I have authored this thesis independently, that I have not used other than the declared sources / resources, and that I have explicitly marked all material which has been quoted either literally or by content from the used sources.

.....
date

.....
(signature)

Abstract

The aim of this diploma thesis is the development of a continuously seeded, continuously operated tubular crystallizer (CSCOTC) and its application for the production of active pharmaceutical ingredients (APIs) and fine chemicals under controlled conditions.

Acetylsalicylic acid (ASA) was crystallized from ethanol (EtOH). It was an optimal model substance because of its noticeable decreasing solubility with falling temperature. An ASA - EtOH seed suspension was fed into the crystallizer system and mixed with a slightly undersaturated ASA - EtOH solution that was kept at elevated temperature. Supersaturation was created via cooling of the crystallizer tubing. Due to its small diameter of only 2 mm, crystallization heat was removed immediately and variations in temperature or concentration did not exist in vertical direction.

Beside the proof-of-concept also the influence of flow rate and seed loading on the product crystal size distribution (CSD) were investigated. Therefore all parameters, such as temperatures and concentrations were held constant while either the flow rate or the seed loading was varied. All experiments resulted in a definite increase of particle size from seed to product crystals. The CSD of all product samples was narrow due to narrow residence time distributions of the suspension and the excellent control of temperature in the tube.

Increasing flow rates led to smaller volume mean diameters because of the decreasing crystallization time available and reduced tendency to agglomeration. Higher seed loading also resulted in smaller volume mean diameters but in a larger number of product crystals.

Additionally, simulation of temperature trajectories and crystal growth were accomplished using MATLAB. The calculated volume mean diameters of the product crystals were all smaller than the ones achieved from the experiment. The reason, however, is that agglomeration is neglected for the calculation.

The concept had been proven feasible and is capable of yielding product masses in a g/min scale.

Kurzfassung

Das Ziel dieser Diplomarbeit war die Entwicklung eines kontinuierlich arbeitenden Rohrkristallisators, um Impfstoffe unter kontrollierten Bedingungen zu Produktkristallen wachsen zu lassen.

Als Modellschubstanz wurde Acetylsalicylsäure (ASA) aus Ethanol (EtOH) auskristallisiert. ASA ist eine ausgezeichnet geeignete Substanz für Kristallisationsversuche, da ihre Löslichkeit mit sinkender Temperatur stark abnimmt und zu einer Übersättigung der Lösung führt. Im Versuchsaufbau wird die mit Impfkristallen beladene Suspension dem Rohrkristallisor zugeführt und mit einer zweiten, leicht unterschättigten ASA-EtOH Lösung gemischt. Durch Kühlen wird Übersättigung der Suspensionslösung erzielt. Der enge Durchmesser des Rohres (2 mm) erlaubt das sofortige Abführen von Kristallisationswärme und verhindert somit ein Temperatur- und Konzentrationsgefälle in vertikaler Richtung.

Zu beweisen war, dass dieser Versuchsaufbau zu den gewünschten Produkteigenschaften führt. Außerdem wurde der Einfluss der Flussrate und der Impfkristallbeladung genauer untersucht. Dafür wurden alle Prozessparameter (Temperaturen, Konzentrationen, etc.) konstant gehalten und jeweils die Flussrate bzw. die Impfkristallbeladung variiert. Alle Versuche führten zu deutlichem Wachstum der Impfkristalle zu Produktkristallen und einer engen Kristallgrößenverteilung, sowie auch zu einer Zunahme an Kristallmasse im g/min Bereich. Die enge Kristallgrößenverteilung kann auf die gut kontrollierbaren Bedingungen und eine enge Verweilzeitverteilung der Kristalle im Rohr zurückgeführt werden.

Durch kürzere Kristallisationszeit bei zunehmenden Flussraten ergaben sich kleinere Produktdurchmesser. Außerdem wurde bei höheren Flussraten die Agglomerationsneigung verringert. Eine steigende Impfkristallbeladung resultierte ebenfalls in kleineren Produktkristallen.

MATLAB wurde verwendet um Temperaturverläufe und Kristallwachstum zu simulieren. Die Ergebnisse wurden verwendet, um den Prozess in Bezug auf Temperaturverläufe zu verbessern.

Danksagung

Zuerst möchte ich mich bei Univ.-Prof. Dipl.-Ing. Dr.techn. Johannes Khinast bedanken, der mir das Schreiben dieser Diplomarbeit am Institut für Prozess- und Partikeltechnik ermöglicht hat.

Besonders möchte ich mich auch bei Dipl.-Ing. Rafael Eder für die gute Betreuung bedanken und die großzügige Unterstützung bei diversen Problemen, wie verspäteten Präsentationen oder verfrühten Prüfungsterminen.

Bei Dipl.-Ing. Dr.techn. Stefan Radl möchte ich mich für die Unterstützung und Geduld in Simulationsfragen bedanken.

Meinen Kollegen danke ich für die großartige Zusammenarbeit und die super Atmosphäre am Institut; insbesondere bei all den "Social Group Meetings and Activities".

Außerdem möchte ich mich bei Desiree bedanken, die mich beim Korrigieren dieser Diplomarbeit unterstützt hat.

Last but not least danke ich ganz besonders meiner Familie, vor allen meinen Eltern und meinem Bruder, und auch meinen Freunden für ihre Unterstützung. Ihr habt mir die letzten Jahre unvergesslich lustig und aufregend gemacht und manch schwierige Situation erleichtert.

Table of Contents

LIST OF FIGURES	III
LIST OF TABLES	VI
ABBREVIATIONS	VII
NOMENCLATURE	VIII
1. INTRODUCTION	1
1.1. MOTIVATION AND GOALS	1
1.2. CONTINUOUS CRYSTALLIZATION OF APIs: STATE OF THE ART	4
2. THEORETICAL BACKGROUND	7
2.1. SUPERSATURATION	8
2.2. NUCLEATION.....	10
2.3. CRYSTAL GROWTH	13
2.4. THERMODYNAMICS VS. KINETICS	16
2.5. PARTICLE SIZE DISTRIBUTION (PSD).....	17
3. SET-UP	19
3.1. MATERIALS & EQUIPMENT	20
4. EXPERIMENTAL	21
4.1. VARIATION OF TOTAL FLOW RATE	21
<i>Experimental Procedure</i>	22
<i>Sampling</i>	23
<i>Sample Characterization</i>	23
<i>Settings</i>	23
4.2. TEMPERATURE PROFILE	24
<i>Simulation of Crystallization via Air Cooling</i>	24
<i>Investigating an Optimized Temperature Profile</i>	24
4.3. VARIATION OF SEED LOADING.....	27
5. MODELS FOR SIMULATION OF GROWTH AND TEMPERATURE	29
5.1. FUNDAMENTAL CALCULATIONS	31
<i>Determining Mass Fractions in the Feed Stream</i>	31
<i>Conduction of Heat through the Tubing</i>	33
5.2. HEAT AND MASS BALANCE.....	33
<i>Overall Mass Transfer Coefficient for ASA Crystals</i>	34
<i>Energy Balance</i>	36
<i>Mass Balance for Dissolved ASA</i>	37
<i>Mass Balance for Solid ASA</i>	37

	<i>Results for a Negligibly Small Heat of Crystallization</i>	38
6.	RESULTS AND DISCUSSION	40
6.1.	VARIATION OF TOTAL FLOW	40
6.2.	TEMPERATURE AND SUPERSATURATION PROFILES	49
	<i>Simulation of Crystallization via Air Cooling</i>	49
	<i>Investigating an Optimized Temperature Profile</i>	51
6.3.	VARIATION OF SEED LOADING.....	53
6.4.	QICPIC VS. MICROSCOPE ANALYSIS	57
7.	CONCLUSION	59
8.	OUTLOOK	61
9.	APPENDIX	62
9.1.	PREPARATION OF SEEDS WITH ASA FROM GL PHARMA	62
9.2.	QICPIC SETTINGS	64

List of Figures

Figure 2-1: The temperature-concentration diagram shows the saturation line dividing into undersaturated (stable) and supersaturated and the metastable limit dividing into metastable and labile zones. Adapted from Mullin, Butterworth-Heinemann, 1992.....	10
Figure 2-2: Supersaturation (including the metastable limits for nucleation) and undersaturation. Adapted from Hofmann, Wiley-VCH, 2004.....	11
Figure 2-3: Free energy versus nucleus radius diagram with the critical nucleus radius r_c . Adapted from Mullin, Butterworth-Heinemann, 1992.....	12
Figure 2-4: Screw dislocation from BCF Model. Adapted from Mullin, Butterworth-Heinemann, 1992.....	15
Figure 3-1: Schema of a continuous operating, tubular crystallizer system. Seed suspension and a solution are mixed in the Y-branch and fed into the coiled crystallizer. The tubing is kept in a box with flushed air to ensure constant ambient temperature. Adapted from Eder et al., Crystal Growth & Design, 2010.....	19
Figure 4-1: Above: Tubular crystallizer with growing crystals. Bottom: Temperature profile along the crystallizer. Agglomeration and Nucleation are neglected. Adapted from Eder et al., Crystal Growth & Design, 2010.....	21
Figure 4-2: Example of how supersaturation changes when system gets rapidly cooled by one water bath.....	25
Figure 4-3: Theoretical example of how supersaturation changes when the system gets rapidly cooled by a number of serially-ordered water baths with decreasing temperatures.....	26
Figure 4-4: Schema of a continuous operating, tubular crystallizer system. Seed suspension and a solution are mixed in the Y-branch and fed into the coiled crystallizer. The tubing is divided into three parts being placed in three water bath for optimized temperature regulation.....	27
Figure 6-1: Crystallization with an ASA-EtOH solution flow of 8.9 mL/min (PI) and 2.5 mL/min of the seed suspension (PII). Top left corner: volume-density distributions of the seeds and two product samples. Top right corner: number	

density distribution of product (sample 2). Bottom: photos of seed and product crystals. <i>Ref.</i> Eder et al., <i>Crystal Growth & Design</i> , 2010	41
Figure 6-2: Crystallization with an ASA-EtOH solution flow of 13.4 mL/min (PI) and 3.8 mL/min of the seed suspension (PII). Top left corner: volume-density distributions of the seeds and two product samples. Top right corner: number density distribution of product (sample 2). Bottom: photos of seed and product crystals. <i>Ref.</i> Eder et al., <i>Crystal Growth & Design</i> , 2010	42
Figure 6-3: Crystallization with an ASA-EtOH solution flow of 17.8 mL/min (PI) and 5.0 mL/min of the seed suspension (PII). Top left corner: volume-density distributions of the seeds and two product samples. Top right corner: number density distribution of product (sample 2). Bottom: photos of seed and product crystals. <i>Ref.</i> Eder et al., <i>Crystal Growth & Design</i> , 2010	43
Figure 6-4: Crystallization with an ASA-EtOH solution flow of 19.7 mL/min (PI) and 5.5 mL/min of the seed suspension (PII). Top left corner: volume-density distributions of the seeds and two product samples. Top right corner: number density distribution of product (sample 2). Bottom: photos of seed and product crystals.	44
Figure 6-5: The average increase of the volume mean diameter from seed to product crystals as a function of flow rate. The mean value of two product samples has been used. Note that the dots, squares and triangles are based on data from different sets of experiments.	48
Figure 6-6: ASA solubility determined with Nývlt (Sol.), dissolved ASA computed according to the model presented in chapter 5 (Calc.) and the resulting supersaturation ratio (S) vs length. <i>Ref.</i> Eder et al., <i>Crystal Growth & Design</i> , 2010	49
Figure 6-7: Temperature (T) with and without heat of crystallization and the increase of the particle diameter (d_p) versus the length of the crystallizer (flow rate = 22.8 mL/min). <i>Ref.</i> Eder et al., <i>Crystal Growth & Design</i> , 2010	50
Figure 6-8: Growth of particles vs crystallizer length. An average of the mean seed diameters was used. Lines show the modeled increase of d_p . <i>Ref.</i> Eder et al., <i>Crystal Growth & Design</i> , 2010	51
Figure 6-9: Supersaturation profile for trial number 1 (1st bath: 8 m, 32 °C; 2nd bath: 7 m, 26 °C) and trial number 2 (1st bath: 5 m, 32 °C; 2nd bath: 10 m, 23 °C).	

In trial 2 the temperature change was too sudden, supersaturation rose too fast at the beginning of the second bath and caused pipe plugging..... 52

Figure 6-10: Supersaturation profile for experiments with air cooling and for trial 4, cooling with 3 water baths. 53

Figure 6-11: q_3 distributions of an average seed sample and of product crystals gained by trials with different seed loadings..... 54

Figure 6-12: The average increase in diameter during the crystallization as a function of seed loading. The mean values of two seed samples and two product samples have been used, respectively..... 55

Figure 6-13: Seeds and product crystals for different seed loadings. Left: product crystals for a loading of *1.2. Right: product crystals for a loading of *2.0..... 56

Figure 6-14: Comparison of microscope analysis and QICPIC analysis for the flow rate experiments..... 58

Figure 9-1: q_3 distribution of ASA raw material from GL Pharma 62

Figure 9-2: q_3 distributions of ASA from GL Pharma after the preparation. Seeds for different seed loading experiments get same particle size distribution..... 63

List of Tables

Table 4-1: Calculated seed loading factor and weighted samples.....	28
Table 5-1: ASA properties: molecular weight MW, density ρ , fusion enthalpy Δh_f and heat capacity c_p	29
Table 5-2: Ethanol properties: molecular weight MW, density ρ , heat conductivity λ and heat capacity c_p	29
Table 5-3: Characteristics of the apparatus: Length L, inner and outer diameter d, the heat conductivity of the tubing λ and the inner and outer heat transfer coefficient α	31
Table 6-1: Results for varying flow rates in a 15 m long tubular crystallizer.	45
Table 6-2: Residence times (t_{res}), Re-Numbers, mass of solid ASA per mL seed-suspension, mass gain (r_m) and the theoretical mass gain ($r_{m,theor}$) of the product to seed crystal masses, temperatures in the Y-fitting (T_{feed}) and the product temperature (T_{prod}) as well as the volume mean diameter ($\bar{d}_{p,vol}$) of the experiment and the calculated crystal diameter ($d_{p,calc}$) and their difference.....	46
Table 6-3: Experiments to find optimized temperature profiles. The data refers to the apparatus shown in Figure 4-4.....	51
Table 6-4: Results for different seed loadings	57

Abbreviations

API	Active Pharmaceutical Ingredient
ASA	Acetyl Salicylic Acid
BCF	Burton-Cabrera-Frank Model
CED	Circle Equivalent Diameter
CSCOTC	Continuously Seeded, Continuously Operated Tubular Crystallizer
CSD	Crystal Size Distribution
CSSD	Crystal Size and Shape Distribution
EMA	European Medicines Agencies
EtOH	Ethanol
FDA	Federal Drug Administration
ICH	International Conference of Harmonization
MIT	Massachusetts Institute of Technology
PI	Pump Flow of Pump I (ASA-EtOH Solution)
PII	Pump Flow of Pump II (Seed Suspension)
PAT	Process Analytical Technology
PSD	Particle Size Distribution
QbD	Quality by Design
SA	Salicylic Acid

Nomenclature

μ	chemical potential [J/mol]
A_p	crystal surface [m ²]
c	concentration [mol/L]
c^*	concentration at equilibrium [mol/L]
c_p	heat capacity [Jkg ⁻¹ K ⁻¹]
d_{20}	density at 20 °C [kg/m ³]
ΔG	total free energy [kJ/mol]
Δh_f	fusion enthalpie [J/mol]
d_{inner}	inner diameter of the crystallizer tubing [m]
d_{outer}	outer diameter of the crystallizer tubing [m]
d_p	particle diameter [m]
$d_{p,0}$	particle diameter of seeds [m]
F_{shape}	shape factor [-]
G	linear growth rate [m/s]
G_L	increase of a characteristic particle length with time (mass dependent) [m/s]
h	step hight [m]
λ	heat conductivity [Wm ⁻¹ K ⁻¹]
L	length of the crystallizer tubing [m]
m	Mass [kg]
\dot{M}	mass flow [kg/s]
MW	molecular weight [g/mol]
N	total number of particles [-]
N/V	concentration of particles in the suspension [L ⁻¹]
$N1, N2, N3$	Nyvit parameters [-]
Q	flow rate [m ³ /s]
$q_0(x)$	number density distribution [μm^{-1}]
$q_3(x)$	volume density distribution [μm^{-1}]
ρ	density [kg/m ³]
R	gas constant [Jmol ⁻¹ K ⁻¹]

r_c	critical radius [m]
Re	Reynolds number [-]
r_m	mass gain [-]
rpm	revolutions per minute [min^{-1}]
S	Supersaturation [-]
T1, T2, T3	temperature of water bath number 1, 2, 3 [$^{\circ}\text{C}$]
T_{amb}	ambient temperature [$^{\circ}\text{C}$]
T_{feed}	feed temperature [$^{\circ}\text{C}$]
t_{res}	residence time [$^{\circ}\text{C}$]
T_{seed}	seed temperature [$^{\circ}\text{C}$]
T_{sol}	solution temperature [$^{\circ}\text{C}$]
V	volume flow [m^3/s]
V_{∞}	step velocity [m/s]
w	mass fraction [kg/kg]
x^*	molar fraction at equilibrium [mol/mol]
y_0	step spacing [m]

1. Introduction

1.1. *Motivation and Goals*

High purity, a narrow particle size distribution (PSD) and low costs are important issues in fields such as fine-chemical, pharmaceutical and food industry.¹⁻⁴ In order to reach these goals, crystallization processes are one of the most common unit operations.⁵⁻¹²

Due to the fact that over 90% of all active pharmaceutical ingredients (APIs) are crystals of small organic molecules, crystallization from solution plays a major role in the pharmaceutical industry.¹³

Objectives in crystallization processes include purity, polymorphism control and crystal size and shape distribution (CSSD).¹⁴⁻¹⁶ Controlling the parameters that affect the aforementioned product characteristics consequently leads to high quality products. This ultimately improves the saleability of the product, as well as the efficiency of the down-stream processes in respect to time and costs.¹⁶ Fine particles or product particles with a broad crystal size distribution (CSD) and a high proportion of small particles in the few μm range slow down filtration unit operations considerably. Additionally washing of the product is less efficient regarding the time needed. Also, more mother liquor, including all impurities present, adhere to the target crystals due to the larger surface to volume ratio of the particles. Moreover, drying becomes very time and energy consuming.¹⁷

Bulk properties, as for example flowability, storage characteristics, segregation phenomena concerning wide CSDs, dusting in the case of fine products and tabletability, are significantly dependent on the product quality in respect to crystal size and CSSD.¹⁸⁻²¹

Especially in the pharmaceutical industry product of highest quality is necessary due to the strict conventions of the regulatory bodies, such as the Federal Drug Administration (FDA) or the European Medicines Agencies (EMA). Here, next to purity, shape and size, as well as CSD are of major importance since these physical properties strongly affect dissolution rates and thus very often the bioavailability of substances.²² Of course the product appearance has to be adjusted to the application. Particles that are inhaled (aerosols) of course require

smaller mean particle diameters than pharmaceuticals that are delivered via oral routes in tablets.

The economic importance of crystalline products, the vast number of diverse substances with considerably varying physical characteristics as well as the different desired bulk properties for the desired target crystals, have resulted in the development of various crystallizer types that are in use nowadays.²³ Differences in the systems are based on how supersaturation, the driving force for crystal growth, is created (i.e. cooling, evaporation, reaction, change in solvent composition etc.⁵), or on the operation mode of the process which can either be batch wise or continuous.

At the moment most unit operations in the pharmaceutical industry are performed batch-wise and this is especially the case for crystallization processes.²⁴ Batch crystallizations offer quite a few advantages for API production, such as the easy implementation and maintenance of the equipment, the ability to use one device for several substances, the suitability for viscous and toxic substances and the ability to grow large crystals.¹⁹ However continuous crystallizations as continuous processes in general, offer significant benefits, including:

- excellent control of process conditions
- eliminating batch to batch variability¹³
- shorter down times
- no scale-up difficulties.¹

Very often smaller equipment can be used for continuous processes even though this may be offset by additional facilities and instrumentation.¹ The crystallizer itself, for example, may be smaller, but several feed- and product tanks could become necessary and thus the overall equipment footprint would be larger.¹ As established above several enormous advantages are associated with continuous production modes. Therefore reactor design for continuous synthesis and crystallizations (e.g., continuously stirred tanks, fluidized or fixed beds and plug-flow reactors etc.) has been excessively used by chemical companies for many decades. However, the pharmaceutical industry has been very reluctant to implement continuous unit operations in the past. In order to take advantage of the positive impacts of continuous processes, a paradigm shift has recently been

recognized and significant efforts towards continuous manufacturing have been initiated by pharmaceutical companies. In the year 2007 Novartis, for example, invested \$ 65 Million in the Massachusetts Institute of Technology (MIT) for the development of continuous manufacturing facilities and processes for pharmaceuticals.²⁴ Economic pressure is rapidly becoming relevant to the pharmaceutical industry and reducing time to market as well as improving process efficiency is becoming important.¹⁶ The Process Analytical Technology (PAT) initiative of the FDA and the Quality by Design (QbD) approach by the International Conference of Harmonization (ICH) is a collaborative effort to introduce new and efficient manufacturing technologies.²⁵ PAT approaches for better process control include systems for design, analysis and control of critical parameters during a process.²⁶ QbD strategies also try to control performances of critical steps in the process in order to ensure final product quality consistency.²⁷ In addition continuous manufacturing modes, employing PAT and QbD strategies, can help to raise efficiency of drug production. Thus, research focusing on continuous crystal production and control is of significant interest to the scientific community and the industry.

The purpose of this work was to establish and test a versatile, continuous crystallizer system that might especially be suitable for applications in the pharmaceutical industry. The underlying principle is the growth of seed-crystals to products in a tubular device with narrow inner dimensions. Due to the small diameter of the tubular crystallizer, the residence time of the suspension (crystals in solution) is very narrow. Therefore the seeds entering the feed end of the tubing simultaneously have approximately the same amount of time for crystal growth. Moreover, the small inner diameter and the large surface to volume ratio of the tubular crystallizer allow for good process control. Thus, spatial variations within the magma (crystals in solution), such as variations of temperature and concentration in the vertical direction, are avoided because the heat of crystallization is removed immediately and mixing in the narrow tube ($d_{\text{inner}} = 2 \text{ mm}$) is not critical. In horizontal direction, however, a smooth trajectory of temperature and concentration can be realized when an optimized cooling gradient is applied. Additionally nucleation events are suppressed by avoidance of rapid cooling and the resulting high levels of supersaturation. The absence of a stirrer that could

cause breakage and attrition of crystals also eliminates fines generation. The narrow residence time of the magma in the pipe, the good process control and the absence of fines generation allow successful achievement of narrow CSDs. The general applicability of this system has already been proven and described in literature by our research group (Eder, Radl & Schmitt et al.).^{1,2}

The experiments presented in the following text utilize acetylsalicylic acid (ASA) as the model-solute and ethanol (EtOH) as the solvent. The ASA – EtOH seed suspension was mixed with a heated, undersaturated ASA-EtOH solution in a Y-branch and the combined feed-stream was fed into the tubular crystallizer. Supersaturation was created via cooling alongside the tubing upon which the seed crystals grew. The impact of parameters, such as flow rate, which is in direct relation to the residence time, as well as seed loading and supersaturation was investigated. Testing the single parameters of interest and their specific influence on the process separately, helped to understand by which factors and how the outcome of the product quantity and quality in respect to CSDs is affected. Additionally simulations concerning the temperature trajectories as well as the concentration gradients and the particle growth have been performed and compared with the experimental results and were used to improve the overall process.

1.2. Continuous Crystallization of APIs: State of the Art

In the pharmaceutical industry continuous crystallization processes are still novel, or even hardly in use,¹³ while their advantages are already exploited in other chemical fields.²⁸ The rising pressure in producing high quality drugs in a cost and time efficient way now directs research and development to a greater extent towards continuous processes.^{23,24} Concepts of continuous crystallizers as being used for large bulk chemicals (e.g., NaCl, KCl and Sugar etc.) are usually not adoptable for crystallization of drug ingredients. Often the throughputs are too large. Moreover, potential operation instabilities may occur.²³ Especially MSMPR or DTB crystallizers show cyclic behavior that results in varying solid mass output and, even worse, in varying CSDs, thus product quality variations.⁵ Hereinafter a

few exceptions for continuous solid API-particle formulations are summarized briefly. For an extended review refer to the quotes given in the text.

Midler et al.²⁹ and Brenek et al.³⁰ for example describe continuous impinging jet precipitations for the generation of micro-particles for use in the pharmaceutical industry. Unfortunately, these impinging jet devices get plugged up very easily. Hence scale up is still rather difficult.¹³

The use of micro-reactor-technology offers typical benefits of continuous operations, such as tight reaction control. Nevertheless, their application has almost exclusively been limited to the production of inorganic nano-particles, but there are several exceptions where organic particles are crystallized. Dombrowski et al.³¹ described the production of lactose crystals by confining the crystallization within drops and Su et al.³² used a microfluidic-based T-junction mixing approach to grow 2,2'-dipyridylamine (DPA) nano-particles in emulsions. Also the patent of Myerson³³ on organic nano-particles offers interesting aspects on crystal engineering in micro-structures for APIs. Gerdts et al.³⁴ dealt with continuous crystallization of proteins within micro-structured channels. Obvious limitations with micro-reactors are the product size and the production rate.²⁴ Although the production rate can be increased via numbering up a certain limitation remains, since excessive high numbers of parallel channels significantly increase the complexity in operation.

Furthermore, the patent by Schiewe and Zierenberg³⁵ illustrates the production of inhalable drug particles in a size range from 0.3-20 μm . Here tube-like channels with alternating non-miscible segments of solution and transport media (e.g., gas or oil) are described. The transport-media prevents the pipe from plugging and a very narrow residence time distribution can be achieved. Also Alvarez and Myerson¹³ recently published an article about antisolvent crystallization of ketoconazole, flufenamic acid and L-glutamic acid in a nonconventional plug flow crystallizer. In this work the influence of supersaturation, by establishing multiple points of antisolvent feeding, was investigated.

In the publication of Méndez del Rio and Rousseau³⁶ a tubular flow-through apparatus with a receiving vessel was used to crystallize paracetamol from ethanolic as well as methanolic solutions. The tube was used to rapidly cool the undersaturated solution below solubility conditions. After primary nucleation crystals grew in the stirred receiving vessel.

The examples established above show that the pharmaceutical industry is finally focusing on the advantages of continuous processes and lately a number of novel crystallization devices have been described in literature. This sufficiently proves that continuous crystallization in pharmaceutical applications is an upcoming research area of increased interest and thus, it was the objective of this work to develop and test a novel, versatile, continuously seeded, continuously operated tubular crystallizer system (CSCOTC).

2. Theoretical Background

The three states of matter are gaseous, liquid and solid. Some substances, such as wax, pitch and glass appear to be solid but yield and flow under pressure. Thus they are occasionally regarded as highly viscous liquids. Basically solids can either be crystalline or amorphous. The difference between crystalline and amorphous matter is the regular arrangement of the molecules, atoms or ions. In crystals the constituents are arranged in fixed and rigid patterns, the so called lattice, resulting in a high level of symmetry and the development of smooth surfaces and definite external crystal faces.^{5,6} Crystallization is an essential technique to separate and purify solid compounds.^{11,37} It is the transfer of substances from an amorphous-solid-, liquid- or gaseous condition into a crystalline state.⁶ The outcome of a crystallization process strongly depends on various factors including level of supersaturation, agitation, impurities (could also be additives if added on purpose e.g. surfactants), type of solvents or solvent mixtures and seeding policy (form, amount). More rapid or stunted growth in given directions and the different relative sizes of crystal faces are the results. In addition the developed faces for a substance also might vary depending on the crystallization process. These factors have an impact on the shape (habit) of the product. The **modification of habit** can be considerably different leading to tabular (platy shape), prismatic or acicular (needle shaped) particles. Since needle shaped or platy particles make the product difficult to handle (filtering, flowability, caking, packing, washing, drying), these shapes are disliked in commercial relevant processes.⁶ Thus it is of utmost importance to control all parameters that affect the outcome of crystallization in order to get products of the highest quality, not only bearing purity in mind.

The second very important aspect in crystallization is **polymorphism and pseudopolymorphism**. Polymorphs refer to different packing arrangements of the same molecules,³⁸ i.e. a chemical substance can crystallize in various different crystal lattices.³⁹ Crystals in which solvate molecules are incorporated into the crystal structure are called solvates and the phenomenon is known as pseudopolymorphism. Whenever water is the solvate, they are called hydrates. The type of polymorph formed depends on the external conditions during the crystallization step.

Different shapes of crystals with the same lattice structure do not lead to different physical behavior of the substance. However, polymorphs show considerably different physicochemical properties,⁴⁰ including solubility and dissolution rate, structural stability, density and melting point. This has an influence on the bioavailability and the shelf life of drugs.^{39,41} Additionally every substance can potentially be polymorphous⁴² and therefore a lot of attention is paid to that polymorphism control. The antipsychotic drug compound aripiprazole, for example, has thus far been reported to crystallize in nine forms including solvates. All of them are protected by patent applications.⁴³ Pharmaceutical companies are well advised to patent every polymorph/pseudopolymorph form of an API possible in order to impede competitors from selling the same substance as another polymorphic form. This is a further reason for focusing on polymorphism.

The continuously seeded, continuously operated tubular crystallizer (CSCOTC) allows good control over process conditions. Therefore it can produce nicely defined, prismatic crystals and agglomerates that allow the free flow of the product. The tubular shaped crystallizer in all probability is a tool for excellent polymorphism control too. The model substance ASA, however, is most likely to crystallize in one form only, even though a second form has been reported in literature.^{44,45}

2.1. Supersaturation

Supersaturation is the driving force for crystallization. Supersaturation ratio (S) is defined as the ratio between the equilibrium concentration (c^*) at a given temperature and a prevailing concentration (c) as shown in Equation 1.^{5,6,11} In this work focus will be on crystallization via cooling. Evaporation of solvent, change of solution composition and chemical reactions are amongst further methods for supersaturation generation, but will not be considered here.

$$S = \frac{c}{c^*}$$

Equation 1

Equation 2 shows that the chemical potential of the solid phase ($\mu_{i,\text{solid}}$) is less than the chemical potential of the solution ($\mu_{i,\text{solution}}$) for supersaturated solutions.

At supersaturation conditions:

$$\mu_{i,solid} < \mu_{i,solution}$$

Equation 2

Thus the system tries to balance this equation by nucleation and/or crystal growth, because a solid phase has to be formed. Figure 2-1 shows a solubility-supersolubility diagram. Generally the graph is divided into a under- and a supersaturated area. In the undersaturated area additional solute still gets dissolved until the equilibrium solubility at a given temperature is reached. The solution remains stable which means no crystallization is possible. Within the metastable zone, however, crystal growth of seeds is possible, but the spontaneous formation of nuclei is improbable. As soon as the metastable limit is crossed and the labile zone is reached, spontaneous nucleation occurs.⁶

Industrial crystallization is usually performed in the metastable zone at moderate levels of supersaturation. The solution becomes supersaturated (e.g., via cooling) and seeds are added subsequently. Thereafter crystal growth consumes the supersaturation. In order to crystallize at constant supersaturation, the cooling is usually adjusted to the crystal surface that is available for crystal growth. Thus the cooling trajectory becomes steeper towards the end of a crystallization batch, because the seeds have already grown and offer, therefore, larger surface areas. Hence supersaturation can be consumed at a faster rate at this state of the crystallization process. For precipitation processes the metastable limit is crossed. High levels of supersaturation are generated in order to get primary nucleation to consume the supersaturation. Many very small particles are the result of such processes.⁵ These phenomena will be detailed in the next chapter.

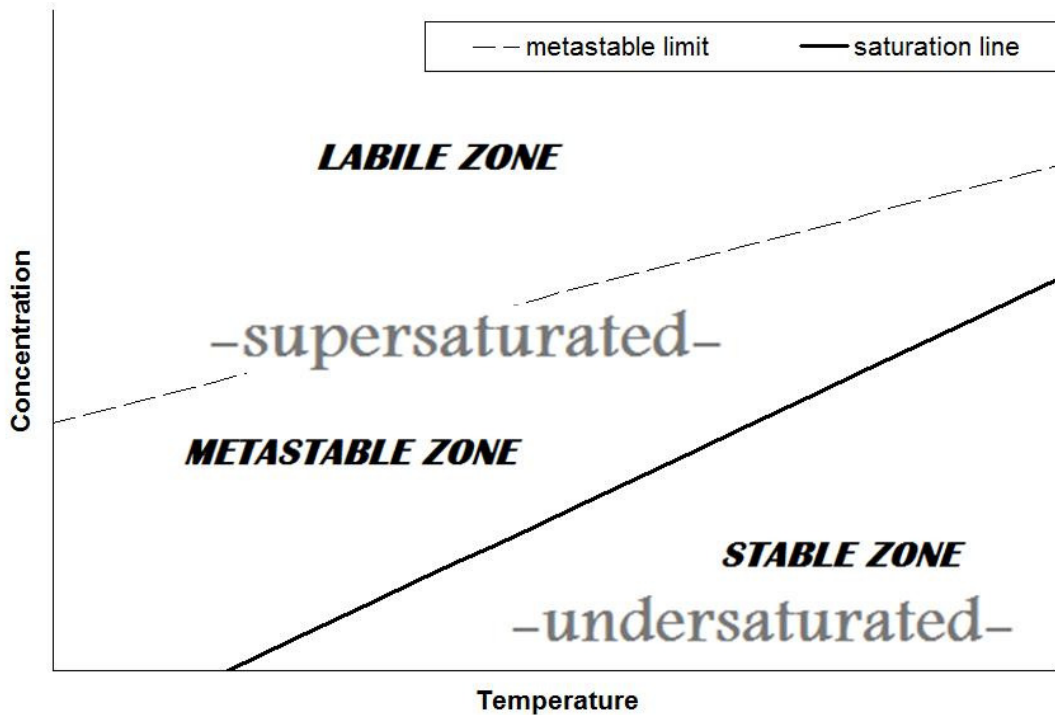


Figure 2-1: The temperature-concentration diagram shows the saturation line dividing into undersaturated (stable) and supersaturated and the metastable limit dividing into metastable and labile zones. Adapted from Mullin, Butterworth-Heinemann, 1992.

2.2. Nucleation

The three types of nucleation described in literature are

- primary homogeneous nucleation,
- primary heterogeneous nucleation
- and secondary nucleation.

In absence of solids, the metastable limit for **primary homogeneous nucleation** must be achieved to get new crystal nuclei. While supersaturation can easily be reached (cooling, solvent evaporation, change of solution composition, reaction etc.), formation of nuclei is a far more complex procedure.⁶ In reality homogeneous nucleation is hard to prove. There is always a chance of having small undetected particles that induce the mechanism as in a heterogeneous process.⁶ If solids in the form of foreign particles (e.g. impurities) or particles of the material being crystallized are present, they affect the rate of nucleation. Either they reduce the free energy of formation necessary and thus accelerate the nucleation, or they

inhibit the process. The former is called **primary heterogeneous nucleation**. In industry primary crystallization should be avoided. Reproduction is rather difficult due to hardly controllable crystal size distributions (CSDs). Hence industrial crystallization is operated in the metastable zone with seeds.¹¹

In the presence of crystals, nucleation already occurs in lower supersaturation regions. This phenomenon is called **secondary nucleation**. Several possible mechanisms for secondary nucleation were already proposed by Strickland-Constable in 1968, such as initial breeding (crystalline dust swept off a newly introduced seed crystal), needle breeding (the detachment of weak outgrowths), polycrystalline breeding (the fragmentation of a weak polycrystalline mass) and collision breeding (a complex process resulting from the interaction of crystals with one another or with parts of the crystallization vessel).⁶

Besides crystal-crystal interactions also contacts between crystals and agitator lead to nucleation through breakage and attrition.¹¹ Here the impeller speed, as well as its relative hardness are in direct proportion to the nucleation rate.⁶

Figure 2-2 comprises the different types of nucleation, as well as the corresponding metastable limits.

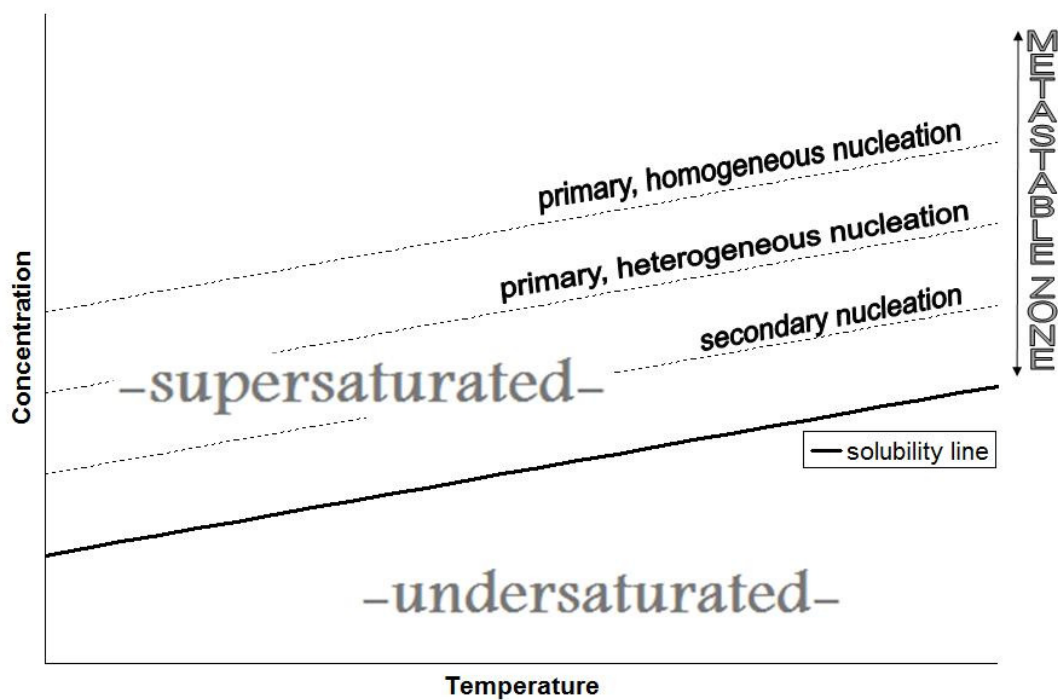


Figure 2-2: Supersaturation (including the metastable limits for nucleation) and undersaturation. Adapted from Hofmann, Wiley-VCH, 2004

As outlined above primary homogeneous nucleation is hard to be observed, since there are always at least small amounts of solid impurities present in solutions. Still the concept is of value for theoretical considerations about nucleation. First supersaturation is necessary to disequilibrate the system (Equation 2). The production of new particles is responsible for rebalancing the supersaturated solution. The concept is that molecules form clusters until a critical size, depending on the conditions (i.e., supersaturation), is reached and a new nucleus is born. The surface energy of the nucleus destabilizes the nucleus but the volume energy contributes to stability. The more molecules are incorporated into a nucleus, the better the volume to surface ratio becomes in favor of the volume. Nuclei being larger than the critical size are then stable and grow. The smaller ones, however, dissolve. Figure 2-3 shows the total free energy (ΔG) as the sum of the surface energy and the volume energy plotted against the cluster radius. The total free energy (ΔG) passes through a maximum with increasing nucleus size, which defines the critical radius (r_c). At this radius and above nuclei are stable.^{5,6,11}

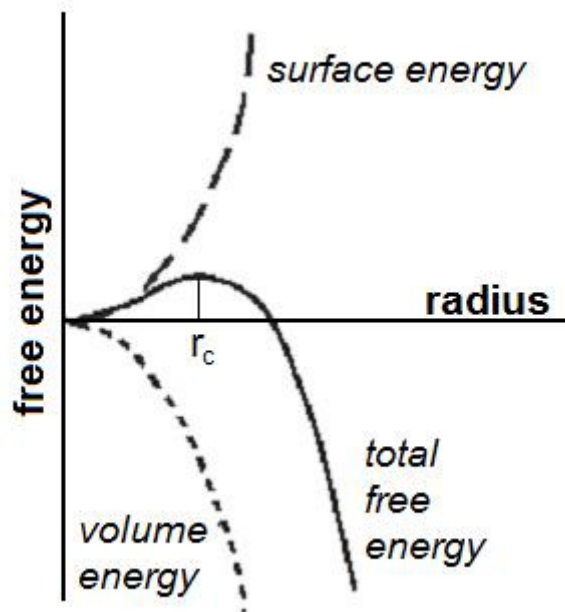


Figure 2-3: Free energy versus nucleus radius diagram with the critical nucleus radius r_c . Adapted from Mullin, Butterworth-Heinemann, 1992.

The work described in this thesis tried to keep nucleation, due to high levels of supersaturation, at a minimum in order to circumvent blockage of the crystallizer

tubing ($d_{\text{inner}} = 2 \text{ mm}$). The principle behind the concept of the CSCOTC is the growth of seed crystals. Crystal growth will be elucidated in the following chapter.

2.3. Crystal Growth

The mass gain of single crystals by solute being incorporated into a crystal surface is called the crystal growth. There are various different theories dealing with the mechanism of crystal growth. Most of them have obvious weaknesses. Thus, they cannot be used in predictive ways for industrial processes. Nevertheless the theories of crystal growth offer good concepts for understanding the mechanisms and phenomena involved in crystal growth and will therefore be explained briefly.

Focusing on a single plane of a crystal is helpful to understand the *linear growth velocity*. The adsorption-theory based on the work of Volmer (1939) suggests a layer by layer growth.^{5,6} In this theory molecules can attach at every location on the surface of a crystal after desolvation, but only at steps or kinks is it possible to incorporate the new molecule into the growing layer. Therefore molecules already attached to the surface must diffuse along the crystal face to a growing step prior to incorporation. The linear growth rate (G) of a face can therefore be expressed as step velocity (V_{∞}), the step height (h), and the step spacing (y_0) (Equation 3).⁵

$$G = \frac{V_{\infty} h}{y_0}$$

Equation 3

Crystal growth rate theories now try to explain where the steps come from and what factors determine the crystal growth rate. The concepts elucidated in the following are

- the two dimensional growth theories (i.e., the monomolecular model, the polynuclear model and the birth and spread model),
- the Burton-Cabrera-Frank (BCF) model including selected derivatives
- and the diffusion layer model.

Two-Dimensional growth theories: The *monomolecular model* suggests the formation of a nucleus that then spreads across the surface at an infinite velocity

till another nucleus is formed. The rate determining step here is the formation of a new two dimensional (2-D) nucleus. In the chapter about nucleation, the formation of a three dimensional nucleus has been discussed. The same concept is applied for the formation of two dimensional nuclei on a crystal surface. As soon as a two dimensional nucleus has been formed the monomolecular model imposes that the layer spreads at infinite velocity across the surface. Thereafter the surface awaits the formation of another nucleus for further growth. This model predicts that larger surfaces will grow at a faster rate since a larger surface is presented for the birth of two dimensional nuclei. This is quite the opposite of what is observed in experiments.⁵

The *polynuclear model* assumes that the spreading velocity of 2-D nuclei is zero. Here the formation of sufficient 2-D nuclei is responsible for the layer formation. But also this approach has its limits. The formation of 2-D nuclei increases with rising supersaturation levels, but at the same time the critical size for 2-D nuclei decreases with rising supersaturation. Therefore the growth rate increases with supersaturation until a maximum is reached. Further supersaturation then results in decrease of crystal growth rates. That behavior has never been observed in experiments either.⁵

In between these approaches of infinite and zero spread velocity, there is the *birth and spread model*. It includes the formation of nuclei and their spreading at a finite constant rate. Additionally 2-D nuclei can form at any given location including incomplete layers.⁵ It does not have the obvious problems of the mono- and polynuclear model, but it is not recommended to use that model in a predictive sense either. All two-dimensional growth theories just work at very low values of surface energy. Otherwise they predict a far too low growth rate at low supersaturation levels.⁵

Burton-Cabrera-Frank (BCF) model: Other approaches work without surface nucleation. The *Burton-Cabrera-Frank (BCF) Model* uses the idea of self-perpetrating steps called screw dislocations shown in Figure 2-4. Therefore the crystal growth is described as a continuous process in contrary to the 2-D growth theories where it depends on nucleation events.

screw dislocation

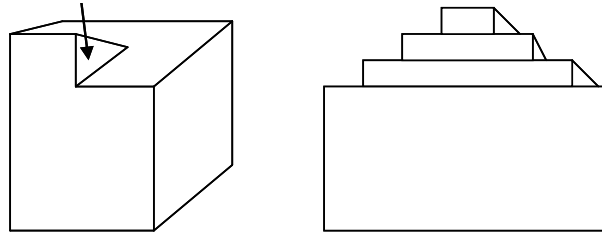


Figure 2-4: Screw dislocation from BCF Model. Adapted from Mullin, Butterworth-Heinemann, 1992.

Whenever a layer is finished the step already entered the next layer and is ready for further growth. The molecules that absorb onto the surface diffuse towards the screw dislocation. Here surface diffusion is rate limiting.⁵ This is usually true for crystal growth in saturated vapor. Whenever bulk diffusion to the surface or the boundary layers respectively is limiting, derivatives of the BCF model are of use. The *Chernov bulk diffusion model* provides a link between crystal growth theories and industrial applicability by considering the BCF model and diffusion in solution, as well as boundary layer thickness and hydrodynamics.

Diffusion layer model: The diffusion layer model simplifies crystal growth and focuses mainly on the diffusion of the solute through the boundary layer between the crystal surface and the bulk solution. The rate limiting facts can either be the diffusion of the solute to the surface or the incorporation of the solute-molecule into the crystal surface.

In industry semi-empirical growth kinetic approaches based on concepts that stem from the theories detailed above, are used to estimate the outcome of a crystallization process or to design a crystallizer in the first place. Equation 4 expresses the relation between supersaturation and crystal growth based on an overall mass increase.⁵

$$R_G = K_g \Delta C^g$$

Equation 4

Here R_G is the increase in crystal mass per unit time and unit area (mass/area time), ΔC the supersaturation, K_g a temperature dependent growth constant and g a number usually between 1 and 2.⁵ To obtain nicely shaped crystals the growth velocity is an essential parameter. The faster the particles develop, the bigger the chance of achieving needles and dendrite-like structures. To have better control over the process and the CSD, a low supersaturation is desirable.^{5,6} Moreover, crystals that grow slow are purer since less impurities are incorporated into the crystal lattice and less mother liquor inclusion deposits are formed. For crystallization processes this implies that an optimum supersaturation level can be found that is defined by acceptable fast growth and excellent product purity, as well as good control of CSD. For the CSCOTC this is a delicate and challenging task due to the short residence time of the crystals in the tube and hence the short time available for crystal growth.¹

2.4. Thermodynamics vs. Kinetics

Nucleation and crystallization not always give the thermodynamic most stable products. Especially when the crystallization rate is high (e.g., due to rapid cooling), less stable products are often the result. Later they are transformed into their thermodynamically more stable polymorphs. Ostwald was the first to generalize this phenomenon in a rule, the *Ostwald's rule of stages*. According to the rule, a system does not transfer to its energetic most stable form without passing some metastable transition stages that resemble its own former state (i.e. the smallest loss of free energy).⁶

It is not possible to find an explanation for this phenomenon by using only thermodynamic approaches. Using crystallization kinetics, however, could give a hint to the fundamental theory.⁶

The rule comes with a large number of exceptions and has never been proven. Due to the countless cases that follow the rule it still plays an important role in chemical industry. Especially when operating in large-scale non-equilibrium processes, the possibility of obtaining another but the thermodynamic most stable product should always be considered.⁶

2.5. Particle Size Distribution (PSD)

Next to purity, polymorphology and shape, particle size and size distribution is one of the most important characteristics of a crystalline product. The CSSD has impact on the bioavailability and on physical properties such as solubility, flowability, dusting, mixing, drying, tableting and dispersing characteristics.^{18,19,21} Hence the product quality and the overall performance of downstream processes, as well as the ability to handle the bulk product, are affected by the CSD. Getting things right during the crystallization step saves money on downstream processes and following up units in the chain of drug formation.^{11,17,22}

Several methods for determining the PSD are available:

- Sieving
- Sedimentation
 - Andreasen
- Optical methods
 - Microscope
 - Light scattering/diffraction
- Non-optical methods
 - Electronic zone sensing (Coulter Counter)
- In-process techniques
- etc.

In general the measuring technique should be chosen according to the sample characteristics. Particle sizes have to be taken into account (e.g., sieving for particle sizes larger 50 μm – except for wet sieving - or laser diffraction for smaller particles <100 μm), as well as shape characteristics. Light scattering technologies for example, require sphere or at least sphere-like particles to get reliable measurement results. Other examples are sedimentation for sedimentation separation processes or microscope analysis for smaller sample sizes. Different methods can give considerably diverse results.

A rather simple principle in determining the PSD is sieving. Particles separated by their size are arranged into classes and evaluated graphically. A mass distribution is obtained. The right handling is described in German standard DIN 66 165.

Microscope analysis is also simple in its functional principle. It uses the area that a particle projects on a surface to determine a significant diameter. Crystals can be viewed and thus shape can be considered without difficulty. This is a big advantage because potential agglomeration can easily be detected. Optical microscopes can analyze particle sizes down to 2 μm . For analysis freeware ImageJ can be used.

Besides microscope analysis also QICPIC® (Sympatec) was used for determining the PSD in this work. It is based on a similar principle as the microscope method but a far larger number of particles can be viewed and evaluated.

Chapter 6.4 compares the microscope analysis with the QICPIC results.

3. Set-Up

Acetyl salicylic acid and ethanol were chosen as model substances. Due to the noticeable decreasing solubility of ASA in ethanol with falling temperature, it is a perfect combination for crystallization experiments. In addition under given conditions ASA crystallizes only in form I although a form II and intermediates have been reported.^{44,45}

An ASA-ethanol seed suspension stream was fed to a Y-branch where it was mixed with an ASA-ethanol solution stream kept at elevated temperature. Figure 3-1 shows the construction.

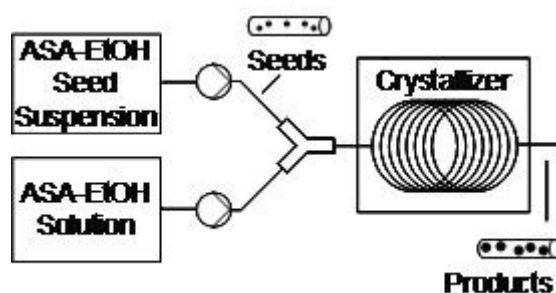


Figure 3-1: Schema of a continuous operating, tubular crystallizer system. Seed suspension and a solution are mixed in the Y-branch and fed into the coiled crystallizer. The tubing is kept in a box with flushed air to ensure constant ambient temperature. Adapted from Eder et al., *Crystal Growth & Design*, 2010

Due to the decrease in temperature and the presence of seeds, crystal growth started right with reaching supersaturation conditions. A 15 m tube with an inner diameter of 2.0 mm was used to continuously grow crystals. Its large surface-to-volume ratio allowed easy removing of the crystallization heat and thus tight temperature control.^{1,35} Furthermore, the narrow residence time distribution obtained leads to narrow crystal size distribution and high quality products.

The tube was kept in a box that was flushed with 3 m³/h pressurized air to avoid temperature increase over time. Product samples were taken at the end and filtrated. The obtained crystals were washed with cyclohexane and dried in a desiccator.

In later experiments three water baths were used instead of the box to create an optimal temperature gradient and thus achieve even better temperature control. Furthermore the influence of cooling characteristics was investigated.

3.1. Materials & Equipment

Acetylsalicylic acid (ASA) (99.0%; $M = 180.16$ g/mol) was purchased from Sigma Life Science for the first set of experiments. Later we used ASA from GL Pharma. Ethanol (EtOH) (99.8%; $M = 46.07$ g/mol, denaturized with 1.0% methyl ethyl ketone) was purchased from Roth (Lactan).

The crystallization set-up uses polysiloxane tubing with a length of 15 m, an inner diameter of 2.0 mm and an outer diameter of 4.0 mm. The solution, as well as the seed suspension was delivered via pumps. For the solution a peristaltic pump (Ismatec BVP- Process IP 65 - 3/6), later referred to as PI, with a PHARMED[®] tubing was used. Its inner diameter was 1.6 mm and its outer diameter was 4.8 mm. The seed suspension was pumped with another peristaltic pump PII (Ismatec Reglo Digital MS 2/6V 1.13C, PHARMED[®] tubing, $d_{\text{inner}} = 2.8$ mm, $d_{\text{outer}} = 5.0$ mm) through a polytetrafluorethylene (PTFE, length = 0.03 m, $d_{\text{inner}} = 1.0$ mm, $d_{\text{outer}} = 3.0$ mm) pipe that was the connection from PII to another short polysiloxane tube ($d_{\text{inner}} = 2.0$ mm, $d_{\text{outer}} = 4.0$ mm) leading to the Y-fitting. The Y-branch was PTFE too with an inner diameter of 2.0 mm.

The seed and product crystal size were determined via picture analysis. Therefore a Leica DM 4000 microscope equipped with a Leica DFC 290 camera was employed. The obtained pictures were edited in ImageJ (<http://rsbweb.nih.gov/ij/>), an open source program. MATLAB was used to illustrate the results. Later QICPIC was used to determine crystal size distributions.

4. Experimental

The principle of continuous crystal growth based on supersaturation via cooling is shown in Figure 4-1. It is provided that flow conditions are ideal, whereas nucleation, particle breakage and agglomeration are neglected.

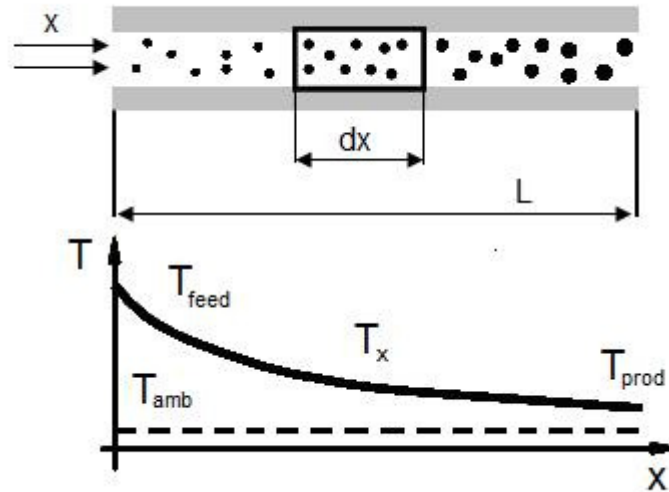


Figure 4-1: Above: Tubular crystallizer with growing crystals. Bottom: Temperature profile along the crystallizer. Agglomeration and Nucleation are neglected. Adapted from Eder et al., *Crystal Growth & Design*, 2010

The feed stream enters at a certain temperature (T_{feed}) that approaches T_{amb} along the temperature trajectory T_x . Due to the small diameter of the tubing, it can be assumed that there is no radial temperature gradient. Crystallization heat is dissipated through a pressurized air stream and in later experiments through a continuous water circulation and cooling in the provided baths. Due to the excellent temperature control and the narrow residence time distribution all entering crystals find the same growth conditions and a narrow CSD can be achieved.

4.1. Variation of Total Flow Rate

For the seed suspension 300 g of ASA from Sigma Life Science and 600 g of EtOH were weighted out into a one liter vessel. To reach the equilibrium the suspension was stirred for at least two days (magnetic stirrer and stir bar).

Dissolution and mechanical effects (including impeller-particle and particle-particle collisions) yielded seeds between 5 and 200 μm .

The same ratio of ASA to Ethanol (200g: 400g) was weighed out for the solution. It was heated up to 62.0 ± 0.2 °C (T_{sol}) to dissolve the whole ASA and used after about 30 minutes. Both, the seed suspension and the ASA-EtOH solution were kept in 1.0 liter storage vessels. While the solution was heated to T_{sol} , the suspension was kept at 24.6 ± 0.2 °C (T_{seed}).

Throughout this set of experiments the flow rates of pump I (ASA-EtOH solution) and pump II (seed suspension) were varied. The ratio between the flows (PI/PII) was always kept constant at 3.5 though.

Solution and seed suspension got mixed in the Y-branch and were led into the crystallizer. Its tubing was coiled on a pipe ($d = 0.1$ m) formed from grid-structured material to ensure good heat transfer with the surrounding air. The coiled up tubing was kept in a box (length 0.41 m, height 0.24 m, width 0.26 m) flushed with 3 m^3/h pressurized air in order to keep the temperature in there (T_{amb}) at 24.3 ± 1 °C.

Experimental Procedure

In order to get the desired flow rates pump I and II had to be calibrated. Therefore the mass flow [g/min] of pump I was determined with EtOH ($d_{20} = 0.79$ g/mL) at 20 °C and was converted into the volume flow [mL/min]. Pump II was calibrated as prescribed by the handbook.

To begin with the seed-suspension was pumped into the crystallizer together with EtOH instead of ASA solution. Seeds had to be present in the tubing at all times to prevent primary nucleation and consequently blockage of the tubing. When seeds had reached the Y-branch, both pumps were stopped and pump II was switched from EtOH to ASA solution. The crystallization got started with the solution reaching the Y-branch.

After about two minutes the first product crystals arrived at the exit of the tubing. A few more minutes were waited to ensure that equilibrium was set. Furthermore, temperatures of seeds, solution and ambience, as well as the suspension temperature at the Y-fitting and the end of the crystallizer were investigated. Then samples were taken.

Sampling

For every run at least three samples were taken. The first one was to characterize the seeds before entering the crystallizer, the others were to determine size and shape characteristics of the product. Seed samples were taken over 60 seconds, whereas enough product was achieved after 30 seconds.

The suspension was filtered under applied vacuum to separate ASA crystals from saturated solution. The samples were washed with cold cyclohexane, an antisolvent, to prevent further agglomeration and dried under vacuum in a desiccator.

Moreover, the mass of product, as well as the mass of the saturated solution and its ASA fraction were determined. Therefore EtOH was evaporated and the left over ASA was weighed out. Hence a mass balance can be made.

Sample Characterization

Pictures of approximately 1000 crystals were taken under microscope. ImageJ, an open source program, was used to estimate the circle equivalent diameter (CED). All pictures were viewed and edited twice in order to exclude overlapped particles. The projected areas of the particles were analyzed and the obtained data was used to generate statistic data, as well as volume and number density distribution graphs in MATLAB.

In addition QICPIC was used to determine particle sizes and distributions. In comparison to MATLAB with QICPIC it was not possible to fit the received data. This analysis was done about 5 months after the actual experiment. It was to compare the different analysis methods and their results. For the results of the variation of flow experiments only MATLAB data is used. The QICPIC data is shown in an additional chapter 6.4, QICPIC vs. Microscope Analysis.

Settings

The crystallizer was operated at five different total flows rates (i.e., ASA + seeded solution) that were, 11.4, 17.2, 22.9, 25.2 and 28.6 mL/min. All other parameters, such as the temperatures of seed suspension and ASA-EtOH solution, the solid loading of the seed suspension, the concentration of the ASA solution, the ratio

between the two feed flow rates – seed suspension and ASA-EtOH solution – and the length of the crystallizer were kept constant.

4.2. *Temperature Profile*

Simulation of Crystallization via Air Cooling

In order to comprehend crystal growth and pipe plugging, the temperature and supersaturation profiles must be known. MATLAB was used to simulate the flow experiments. The model used for MATLAB is described in chapter 5, Models for Simulation of Growth and Temperature.

Investigating an Optimized Temperature Profile

A constant supersaturation within the metastable zone is desirable to achieve uniform crystal growth. By rapidly cooling a system disequilibrates and supersaturation rises. The development of crystals consumes the surplus dissolved substance and leads the liquid phase back to equilibrium conditions.

A rapid increase in supersaturation leads to high crystal growth rates, usually at the expense of shape and purity of crystals. The faster crystals increase in size, the more impurities get enclosed. Also the formation of perfect crystals needs time and therefore prefers a constantly lower value of supersaturation.

Figure 4-2 shows an example of how the supersaturation profile is affected by temperature change and crystal size increase. Here a continuous crystallizer tubing is cooled by one single water bath from 37 °C down to 32 °C and high supersaturation values up to 1.28 are achieved. The profile passes through a supersaturation maximum because crystal growth rebalances and thus decreases the supersaturation. In order to avoid the above mentioned impurities and shape weaknesses a profile more like Figure 4-3 would be desirable.

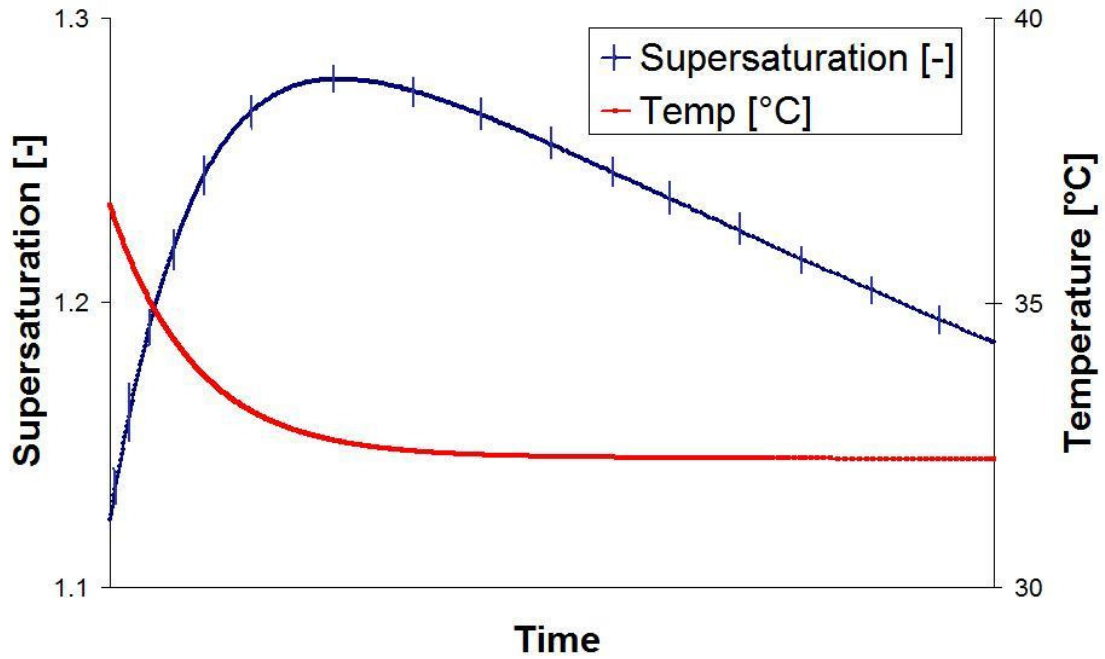


Figure 4-2: Example of how supersaturation changes when system gets rapidly cooled by one water bath

A slightly undersaturated suspension enters the crystallizer tubing and supersaturation is built up with decreasing temperature. The surplus of the dissolved ASA is consumed and supersaturation decreases again (Figure 4-2). To obtain the supersaturation curve from Figure 4-3 an endless number of water baths would be necessary. Whenever the supersaturation value starts to fall a subsequent cooling bath with lower temperature than the one before lowers the solubility of ASA in ethanol and thus reincreases the supersaturation.

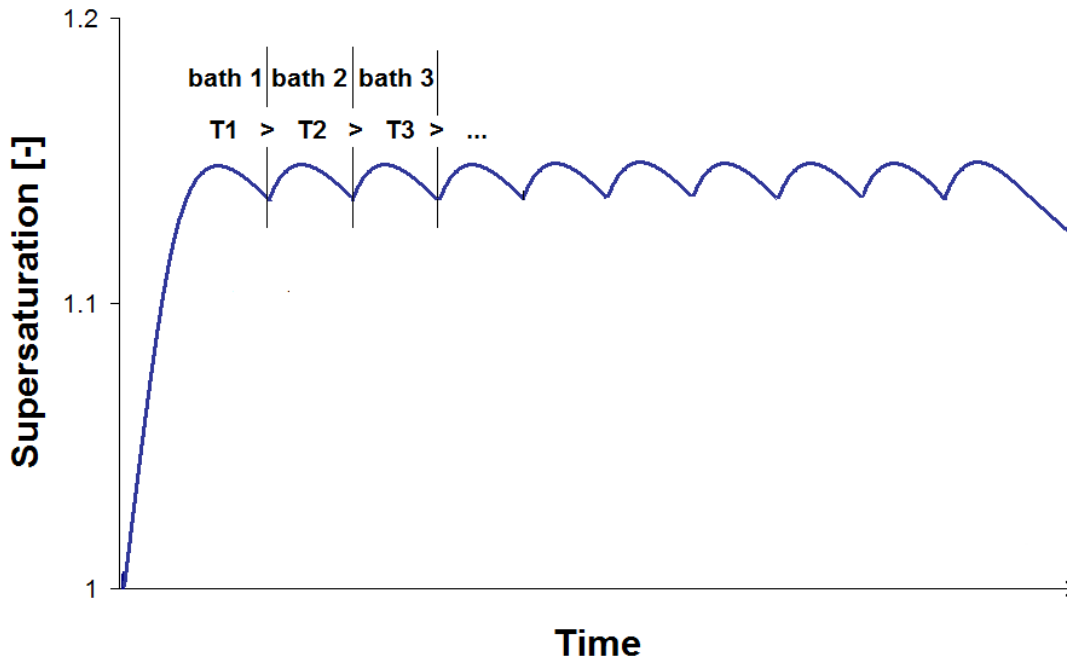


Figure 4-3: Theoretical example of how supersaturation changes when the system gets rapidly cooled by a number of serially-ordered water baths with decreasing temperatures.

In Figure 4-3 saturation is getting close to constant without big maxima. Hence the risk of pipe plugging due to nucleation effects is reduced and the number of impurity inclusions decreases. Due to the high instrumental expense, it makes absolute sense to strike a balance between these operating possibilities. For the realization of this concept, the device shown in Figure 4-4 was implemented. The 15 m crystallizer tubing was separated between two and later three additional water baths with one having lower temperature than the one before ($T_1 > T_2 > T_3$). Future objectives must be the implementation of counter- and cross current cooling flows that would definitely be appropriate for industrial applications. Thus a smooth temperature profile and a more constant supersaturation profile can be achieved.

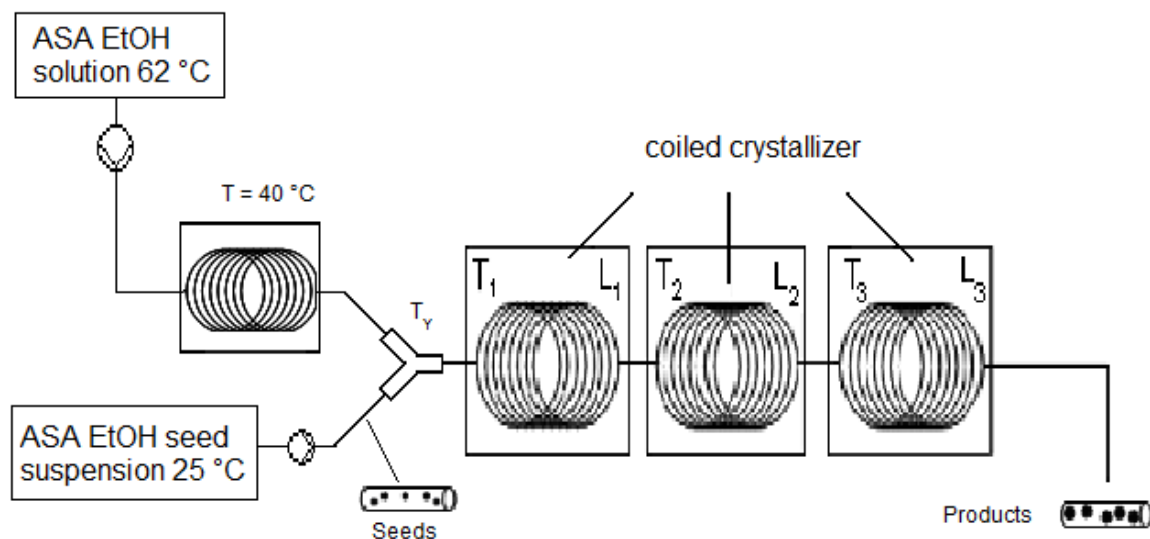


Figure 4-4: Schema of a continuous operating, tubular crystallizer system. Seed suspension and a solution are mixed in the Y-branch and fed into the coiled crystallizer. The tubing is divided into three parts being placed in three water bath for optimized temperature regulation.

An optimized temperature profile, closer to crystallization at constant supersaturation, was requested to improve the crystallization of ASA from EtOH. For determining this temperature profile a strict control of all temperatures was necessary. Therefore the seed suspension was put into a water bath that was held at 25 °C. The solution temperature was set 40 °C with another bath right before the Y-branch. The optimal adjustments concerning the lengths of the tubings and temperatures in the baths were achieved empirically. In addition MATLAB was used to reconstruct the temperature gradient, the supersaturation and the crystal growth with varying operating parameters. A combination of experiments and simulations led to the adjustments that improved the crystallization process.

4.3. Variation of Seed Loading

For this set of experiments ASA from GL Pharma was used and seeds were prepared as described in the Appendix.

The principle of this trial and the basic data is the same as in the variation of flow experimental series. Here, however, we chose a constant total flow of 16.9 mL/min and varied the seed loading by variation of the amount of ASA in the seed

suspension. Moreover, the in chapter 4.2 investigated temperature profile was retained (see Figure 4-4).

The seed loading and its sample weight were pre-calculated using the Nývlt Equation 5. The molar fraction of ASA at equilibrium, x^* , can be calculated with the Nývlt parameters. For an EtOH solution the parameters for Equation 5 are $N_1 = 27.769$, $N_2 = -2500.906$ and $N_3 = -8.323$.⁴⁶ The temperature T has the unit Kelvin [K].

$$\log x^* = N_1 + \frac{N_2}{T} + N_3 \cdot \log T \quad \text{Equation 5}$$

The primary seed loading (300 g ASA in 600 g EtOH) was set factor 1, which was 0.766 mol ASA solid at 25 °C. The multiplication factors shown in Table 4-1 were weighted out for further runs.

Table 4-1: Calculated seed loading factor and weighted samples

calculated seed loading factor	weighted sample ASA	weighted sample EtOH
[-]	[g]	[g]
*1.0	300	600
*1.2	273	500
*1.5	308	500
*1.7	331	500
*2.0	365	500

The start up for the runs and the sampling were the same as in the variation of flow experiments (see chapter 4.1). In addition a second seed sample was taken at the end of each trial to monitor the seed size. This was due to initial problems with seed preparation and establishment of equilibrium.

Sample characterization was done by the use of QICPIC.

5. Models for Simulation of Growth and Temperature

The models described in this chapter have been developed for a recent publication of our research group.¹

To predict the temperature profile, the particle size, the supersaturation level and the dissolved ASA mass fraction during crystallization in a tubular crystallizer a model for a MATLAB calculation has to be established. Therefore two major assumptions have to be made:

- Only a single particle size d_p is used to describe particles at each point x within the crystallizer.
- A constant number of particles is assumed and hence agglomeration and breakage have to be neglected.

This leads to a simplification of the mass and energy balance equations as shown later.

Physicochemical data for ASA and EtOH used are listed in Table 5-1 and Table 5-2. Additional data needed for further calculations is provided in the text explaining the respective equations.

Table 5-1: ASA properties: molecular weight MW, density ρ , fusion enthalpy Δh_f and heat capacity c_p .

MW_{ASA} [g/mol]	ρ_{ASA} [kg/m ³]	$\Delta h_f^{46,47}$ [J/mol]	$c_{p,ASA}^{47}$ [J/kgK]
180.16	1350	29800	1260

Table 5-2: Ethanol properties: molecular weight MW, density ρ , heat conductivity λ and heat capacity c_p .

MW_{EtOH} [g/mol]	ρ_{EtOH} [kg/m ³]	λ_{EtOH} [W/mK]	$c_{p,EtOH}$ [J/kgK]
46.07	790	0.1676	2400

The later needed heat of crystallization (Δh_{cryst}) can be equated with the negative value of the fusion enthalpy (Δh_f). Moreover, Δh_{cryst} is assumed constant over the whole temperature and concentration profile of the crystallizer.

As a further assumption the heat conductivity of the ASA – EtOH suspension ($\lambda_{\text{ASA-EtOH}}$) was set equal to the heat conductivity of pure EtOH (λ_{EtOH}).

For the calculation of the dissolved ASA during the crystallization process the Nývlt model (Equation 5) is used.⁴⁶

Varying settings such as flow rates (Q_{solution} , Q_{seed}), seed and solution temperatures (T_{seed} , T_{solution}), ambient temperature (T_{amb}), masses of ASA and EtOH in seed suspension and ASA-EtOH solution ($m_{\text{EtOH,solution}}$, $m_{\text{EtOH,seeds}}$, $m_{\text{ASA,solution}}$, $m_{\text{ASA,seeds}}$), as well as the particle diameter of the seeds ($d_{p,0}$) are adjusted as provided in the particular experiments. While the seed temperature depended on the room temperature during the variation of flow experiments, it was kept constant at 25 °C for the other trials. The same is for the ambient temperature. During the first sets of experiments the ambient temperature was room temperature. Later the ambient temperature was the adjusted temperature of the respective water baths. The solution temperature was 62 °C. While for the variation of flow experiments the temperature was measured again before the Y-branch, another water bath was used for the other experiments to keep the temperature at 40 °C before entering the branch. The combination of seed and solution temperature with the flow rates gives the actual feed temperature (T_{feed}).

Due to pretty constant particle diameters with the ASA from Sigma Life Science in the variation of flow experiments and to simplify the comparison of the different growth profiles, the seed particle diameter for these first experiments was set at $d_{p,0} = 114 \mu\text{m}$. This is an average of the volume mean diameters of all seeds from the experiments listed in Table 6-1.

As shape factor F_{shape} used for the calculations is 1 [-].

Table 5-3 lists the characteristics of the tubing of the continuous crystallizer: The total length (L), the inner and outer diameter (d_{inner} , d_{outer}), the heat conductivity of the tubing (λ_{tubing}), the inner heat transfer coefficient (α_{inner}), as well as the outer heat transfer coefficients for ambient air ($\alpha_{\text{outer, air}}$) and water ($\alpha_{\text{outer, water}}$). These last two values have been determined empirically. The α_{inner} of 306 W/m²K is valid for a pipe with an inner diameter of 0.002 m where the heat conductivity of pure EtOH

($\lambda_{\text{EtOH}} = 0.1676 \text{ W/mK}$ at 300 K)⁴⁸ has been used for the ASA-EtOH suspension in the crystallizer.

Table 5-3: Characteristics of the apparatus: Length L, inner and outer diameter d, the heat conductivity of the tubing λ and the inner and outer heat transfer coefficient α .

L [m]	d _{inner} [m]	d _{outer} [m]	λ_{tubing} [W/mK]	α_{inner} [W/m ² K]	$\alpha_{\text{outer, air}}$ [W/m ² K]	$\alpha_{\text{outer, water}}$ [W/m ² K]
15	0.002	0.004	0.3	306	70	1494

As the Reynolds numbers in Table 6-2 show (i.e., $Re \ll 2300$) a laminar, thermally fully developed flow in the tubing can be assumed. In addition the wall temperature is assumed to be constant and the Nusselt number (Nu) is constant and equal to 3.651 [-].⁴⁸

For the calculations with more than one ambient temperature (two to three water baths with different temperatures) the calculations have been done separately for the particular baths. All settings have been adapted for the respective water bath. Therefore results from the first part of the tubing within the first water bath have been employed as start characteristics for the second bath. The crystal diameter (d_p) at the end of the first bath has been used as an inlet parameter for the second tubing part instead of the primary seed diameter ($d_{p,o}$). Also feed temperatures have been adapted from the previous results. In the end the obtained results for the baths have been pieced together and give the profiles for the total 15 [m] crystallizer.

5.1. Fundamental Calculations

Determining Mass Fractions in the Feed Stream

The mass fraction of undissolved ASA (w_{solid}) is based on the total mass fraction ASA (w_{ASA}) and the mass fraction of the ASA dissolved in the feed stream ($w_{\text{Diss,feed}}$).

$$w_{ASA} = w_{solid} + \frac{m_{Diss,feed}}{m_{susp}} \quad \text{Equation 6}$$

$$w_{Diss,feed} = \frac{m_{Diss,feed}}{m_{liqPhase,feed}} \quad \text{Equation 7}$$

$$w_{Diss,feed} = \frac{w_{Diss,seed} \cdot (1 - w_{solid,seed}) \cdot \dot{m}_{seed} + w_{EtOH} \cdot \dot{m}_{EtOH}}{(1 - w_{solid,seed}) \cdot \dot{m}_{seed} + \dot{m}_{EtOH}} \quad \text{Equation 8}$$

Here $w_{Diss,seed}$ is the saturated mass fraction of dissolved ASA in the seed stream, $w_{solid,seed}$ is the mass fraction of solid ASA in the seed stream and w_{EtOH} is the mass fraction of ASA in the ASA-EtOH solution. m_{susp} refers to the total mass flow of the feed suspension including ASA solid, ASA dissolved and EtOH in the feed, whereas $m_{Diss,feed}$, $m_{liqPhase,feed}$, m_{seed} and m_{EtOH} refer to the mass flows of dissolved ASA in the feed stream, the liquid-phase mass flow in the feed, the total mass flow rate of the seed and the total mass flow rate of the ASA-EtOH solution, respectively.

Combining Equation 6 and Equation 7 leads to the mass fraction of solid ASA (w_{solid}) as shown below.

$$w_{solid} = \frac{w_{ASA} - w_{Diss,feed}}{1 - w_{Diss,feed}} \quad \text{Equation 9}$$

With the mass flow rate of solid ASA in the feed (m_{solid}), the mass of a single particle (m_p) and the volume flow of the feed suspension (\dot{V}) the concentration of particles (N/V) can be calculated:

$$\frac{N}{V} = \frac{\dot{m}_{solid}/m_p}{\dot{V}} = \frac{\dot{m}_{solid}/m_p}{\dot{m}_{susp}/\rho_{susp}} = \frac{w_{solid} \cdot \rho_{susp}}{d_{p,seed}^3 \cdot \pi/6 \cdot \rho_{ASA}} \quad \text{Equation 10}$$

ρ_{susp} and ρ_{ASA} are the densities of the suspension and the pure ASA, whereas the suspension density was calculated from the densities of the pure substances and the mass fraction in the suspension. $d_{p,seed}$ is the diameter of a single seed particle.

Conduction of Heat through the Tubing

The total heat transfer rate \dot{Q} based on the outer surface of the pipe is given by Equation 11. While L is the length of the pipe and r_{outer} the outer radius, T is the suspension temperature in the pipe and T_{amb} the ambient temperature.

$$\dot{Q} = 2 \cdot \pi \cdot r_{outer} \cdot L \cdot k \cdot (T - T_{amb}) \quad \text{Equation 11}$$

Considering the thickness of the pipe, the total heat transfer coefficient k can be calculated as follows:

$$k = \frac{1}{r_{outer} \cdot \left(\frac{1}{r_{inner} \cdot \alpha_{inner}} + \frac{\ln(r_{outer}/r_{inner})}{\lambda_{tubing}} + \frac{1}{r_{outer} \cdot \alpha_{outer}} \right)} \quad \text{Equation 12}$$

Here, α_{inner} and α_{outer} refer to the heat transfer coefficient on the inside and the outside of the pipe and λ_{tubing} is the heat conductivity of the pipe material. r_{inner} and r_{outer} are the inner and outer radius of the tubing.

5.2. Heat and Mass Balance

Before setting up equations for the heat and mass balance of a tubular crystallizer (i.e., a pipe reactor) a few assumptions have to be taken into account:

- steady-state conditions for the crystallizer are required
- the density of the suspension (ρ_{susp}) is constant
- no mixing in axial direction but perfect radial mixing
- particles and the liquid phase of the suspension have locally the same temperature (T)
- the heat transfer coefficient from the suspension to the tubing and to the ambient air (or water bath) is constant. The ambient temperature (T_{amb}) is constant.

- the specific heat of crystallization (Δh_{cryst}) is equal to the value of the heat of fusion of ASA (Δh_f) and constant for the whole length of the crystallizer
- the heat capacity of the suspension is constant and can be calculated as follows:

$$\dot{m}_{\text{tot}} \cdot c_{p,\text{tot}} = \dot{m}_{\text{EtOH}} \cdot c_{p,\text{EtOH}} + \dot{m}_{\text{ASA}} \cdot c_{p,\text{ASA}} \quad \text{Equation 13}$$

Here, \dot{m}_{tot} , \dot{m}_{EtOH} , and \dot{m}_{ASA} are the total mass flow rate, the mass flow rate of the EtOH solution and the solid ASA mass flow in the feed stream, respectively. $c_{p,\text{tot}}$, $c_{p,\text{EtOH}}$ and $c_{p,\text{ASA}}$ denote the specific heat capacities of the total feed, the EtOH solution and the solid ASA.

Overall Mass Transfer Coefficient for ASA Crystals

There are two phenomena that control the growth of ASA particles: the mass transfer (i.e., diffusion of ASA to the surface of a crystal) or the surface integration. Although both are very complex a number of models dealing with the overall growth rate (considering diffusion as well as surface integration of ASA) can be found in literature. Typically power law models describing the increase of a characteristic particle length (i.e., the mean diameter) with time are used.^{7,49,50} Here G_L refers to the growth rate.

$$G_L = K_{g,L}(T) \cdot \Delta w^g \quad \text{Equation 14}$$

$K_{g,L}$ is a temperature dependent parameter and g a dimensionless exponent. Δw characterizes the influence of the mass fraction, a driving force on the growth rate. For ASA crystallization g becomes equal to unity⁷ and the G_L equation for ASA can be written as follows:

$$G_L = \frac{d(d_p)}{dt} = K_{g,L} \cdot \Delta w \quad \text{Equation 15}$$

Granberg et al.⁵⁰ documented the parameter $K_{g,L}$ for the crystallization of paracetamol from an acetone-water mixture in the range of 10^{-5} to 10^{-4} m/s. For the system ASA-EtOH it is expected the same order of magnitude.

Equation 16 explains the relation between the growth rate of the mean particle diameter d_p and the mass growth rate.

$$\frac{d(d_p)}{dt} = \frac{2}{\rho_{ASA} \cdot A_p} \cdot \frac{dm_p}{dt} \quad \text{Equation 16}$$

$$\frac{d(m_p)}{dt} = \dot{M}_{cryst} = A_p \cdot K_g \cdot \rho_{sol,sat} \cdot \Delta w \quad \text{Equation 17}$$

Here \dot{M}_{cryst} is the total rate of crystallization and $\rho_{sol,sat}$ is the saturated solution density and assumed to be equal to the density of pure EtOH. K_g is an overall mass transfer coefficient that takes the mass transfer and the integration of dissolved ASA onto the crystal surface A_p into account. The relation between K_g and $K_{g,L}$ is given as follows:

$$K_{g,L} = 2 \cdot \frac{\rho_{sol,sat}}{\rho_{ASA}} \cdot K_g \quad \text{Equation 18}$$

The ratio of the saturated solution density, $\rho_{sol,sat}$, to the density of solid ASA, ρ_{ASA} , for the ASA-EtOH system is 0.59. According to the literature data of Lindenberg et al.⁷ $K_{g,L}$ follows Equation 19 for ASA. $K_{g,L1}$ is 0.321 m/s (using [g/kg] as a measure for the solubility of ASA) and $K_{g,L2}$ is $2.58 \cdot 10^4$ J/mol.

$$K_{g,L} = K_{g,L1} \cdot \exp\left[-\frac{K_{g,L2}}{R \cdot T}\right] \quad \text{Equation 19}$$

Substituting into Equation 19 yields $K_{g,L} = 1.2 \cdot 10^{-5}$ m/s and consequently $K_g = 1.0 \cdot 10^{-5}$ m/s for 305 K as an average temperature in the tubular crystallizer.

Energy Balance

The differential energy balance is:

$$\dot{m}_{tot} \cdot c_{p,tot} \cdot (T(x) + dT) = \dot{m}_{tot} \cdot c_{p,tot} \cdot T(x) + \dot{q}_{cryst}(x) \cdot dx \cdot d_{inner}^2 \cdot \pi/4 - dx \cdot d_{outer} \cdot \pi \cdot k \cdot (T(x) - T_{amb})$$

Equation 20

The volumetric heat source \dot{q}_{cryst} due to crystallization can be calculated as:

$$\dot{q}_{cryst}(x) = -\dot{m}_{cryst} \cdot \Delta h_{cryst}$$

Equation 21

The volumetric rate of crystallization \dot{m}_{cryst} is given in Equation 22.

$$\dot{m}_{cryst} = \frac{d\dot{M}_{cryst}}{dV} = \frac{4 \cdot N \cdot d_p^2 \cdot F_{shape} \cdot K_g \cdot \left(\frac{w_{Diss}}{1/\rho_{EtOH} + w_{Diss}/\rho_{ASA}} - \rho_{ASA,sat}(T) \right)}{L \cdot d_{inner}^2}$$

Equation 22

Here $d\dot{M}_{cryst}$ refers to the total rate of crystallization in the differential volume dV , F_{shape} is the shape factor and here assumed equal to unity (as for perfect spheres) and K_g is the mass transfer coefficient of ASA in the EtOH solution. Moreover, ρ_{EtOH} is the density of pure EtOH and $\rho_{ASA,sat}(T)$ is the partial saturation density of ASA at a certain temperature T . It is based on the equilibrium mole fraction and the densities of the components.

For the final differential equation for the temperature profile we now get Equation 23.

$$\frac{dT}{dx} = \frac{d_{outer} \cdot \pi}{\dot{m}_{tot} \cdot c_{p,tot}} \cdot (T(x) - T_{amb}) \cdot k \left(\frac{N \cdot K_g \cdot F_{shape} \cdot \Delta h_{cryst} \cdot \left(\frac{w_{Diss}}{1/\rho_{EtOH} + w_{Diss}/\rho_{ASA}} - \rho_{ASA,sat}(T) \right)}{L \cdot d_{outer}} \right) \left(\frac{d_p^2}{[k \cdot (T(x) - T_{amb})] - 1} \right)$$

Equation 23

Mass Balance for Dissolved ASA

For dissolved ASA the mass balance equation is given below.

$$dw_{Diss} = - \frac{d\dot{M}_{cryst}}{\dot{m}_{EtOH}}$$

Equation 24

Combining this equation with the expression for the total rate of crystallization in the differential volume dV we obtain:

$$\frac{dw_{Diss}}{dx} = - \frac{1}{\dot{m}_{EtOH}} \cdot \frac{N}{L} \cdot d_p^2 \cdot \pi \cdot K_g \cdot F_{shape} \cdot \left[\frac{w_{Diss}}{1/\rho_{EtOH} + w_{Diss}/\rho_{ASA}} - \rho_{ASA,sat}(T) \right]$$

Equation 25

The boundary condition for this equation is the dissolved ASA mass fraction in the feed stream as given in Equation 8.

Mass Balance for Solid ASA

The differential change in particle mass (neglecting breakage and agglomeration) can be calculated as follows:

$$d(m_p) = \dot{M}_{cryst} \cdot dt = d_p^2 \cdot \pi \cdot F_{shape} \cdot K_g \cdot \left[\frac{w_{Diss}}{1/\rho_{EtOH} + w_{Diss}/\rho_{ASA}} - \rho_{ASA,sat}(T) \right] \cdot \frac{dx}{v}$$

Equation 26

Here v refers to the mean velocity of the suspension. Further can be stated:

$$d(m_p) = \frac{d_p^2 \cdot \pi}{2} \cdot d(d_p) \cdot \rho_{ASA} \quad \text{Equation 27}$$

Thus, we obtain the following differential equation for the evolution of the particle diameter along the axial coordinate of the tubular crystallizer.

$$\frac{d(d_p)}{dx} = \frac{2 \cdot K_g \cdot F_{shape} \cdot \left[\frac{w_{Diss}}{1/\rho_{EtOH} + w_{Diss}/\rho_{ASA}} - \rho_{ASA,sat}(T) \right]}{\dot{Q}_{feed} / (d_{inner}^2 \cdot \pi/4) \cdot \rho_{ASA}} \quad \text{Equation 28}$$

\dot{Q}_{feed} is the volume flow rate of the feed suspension entering the crystallizer. The boundary condition for this equation is given by the seed particle diameter $d_{p,0}$.

Results for a Negligibly Small Heat of Crystallization

For $\Delta h_{cryst} = 0$ the following expression for the temperature profile $T(x)$ can be assumed:

$$\Phi(x) = \frac{T_{feed} - T(x)}{T_{feed} - T_{amb}} = 1 - \exp \left[- \frac{k \cdot x \cdot d_{outer} \cdot \pi}{\dot{m}_{tot} \cdot c_{p,tot}} \right] \quad \text{Equation 29}$$

$\Phi(x)$ refers to the dimensionless temperature difference between the feed (T_{feed}) and the suspension temperature (T_x) at the axial distance x from the inlet. Rewriting Equation 29 gives the equation for the total heat transfer coefficient k from experiments involving, e.g., water:

$$k = -\ln \left(1 - \frac{T_{feed} - T_{prod}}{T_{feed} - T_{amb}} \right) \cdot \frac{\dot{m}_{tot} \cdot c_{p,tot}}{L \cdot d_{outer} \cdot \pi} \quad \text{Equation 30}$$

T_{prod} is the temperature exiting the tubular crystallizer and T_{amb} the ambient temperature. The outer heat transfer coefficient can be estimated as follows:

$$\alpha_{\text{outer}} = \frac{1}{\left(\frac{1}{r_{\text{outer}} \cdot k} - \frac{\ln(r_{\text{outer}}/r_{\text{inner}})}{\lambda_{\text{tubing}}} - \frac{1}{r_{\text{inner}} \cdot \alpha_{\text{inner}}} \right)} \cdot r_{\text{outer}}$$

Equation 31

6. Results and Discussion

6.1. *Variation of Total Flow*

The results given and discussed here will be microscope results only, because at this point in time QICPIC was not available. These results have already been published by Eder et al.¹

Four of the five different total flows were chosen for detailed study.

Figure 6-1 shows the volume-density distribution $q_3(x)$ of the seeds and two product samples for a total flow rate of 11.4 mL/min. An increase in volume through crystal growth is clearly detectable and can also be seen in the microscopic pictures. In addition agglomeration and crystal intergrowth occur but still are not the primary reason for the enlargement.

The two product samples give very similar distributions. This means that equilibrium has already been reached. Moreover, the CSD is rather narrow which testifies to good product quality.

On the upper right corner of the figure, the number density distribution $q_0(x)$ of the product (sample 2) is illustrated. It makes clear that no fines have been produced.

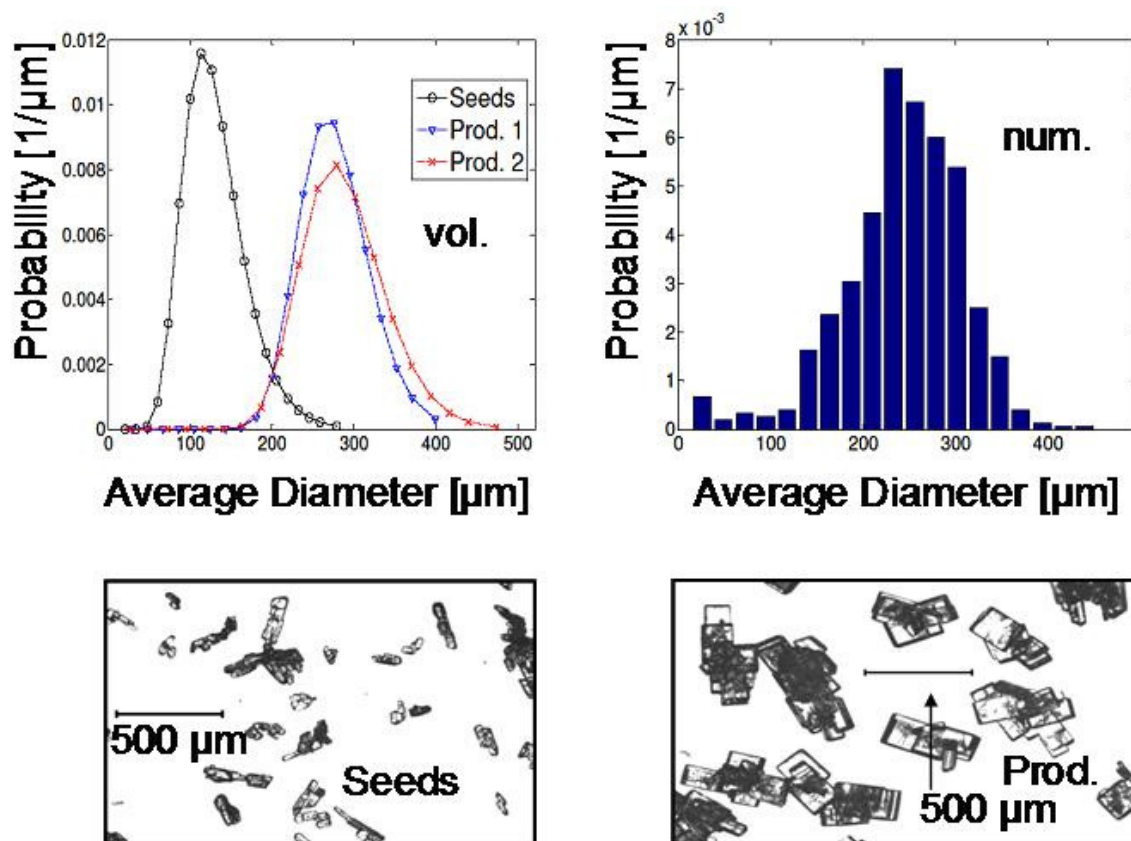


Figure 6-1: Crystallization with an ASA-EtOH solution flow of 8.9 mL/min (PI) and 2.5 mL/min of the seed suspension (PII). Top left corner: volume-density distributions of the seeds and two product samples. Top right corner: number density distribution of product (sample 2). Bottom: photos of seed and product crystals. *Ref.* Eder et al., *Crystal Growth & Design*, 2010

In Figure 6-2 and Figure 6-3 the distributions for the flow rates of 17.2 and 22.8 are shown. The volume distribution graphs also demonstrate a definite crystal growth during their residence time in the tubular crystallizer. Compared to the first flow, one can already tell that with higher flow rates and resulting lower residence time the product crystals emerge a little smaller.

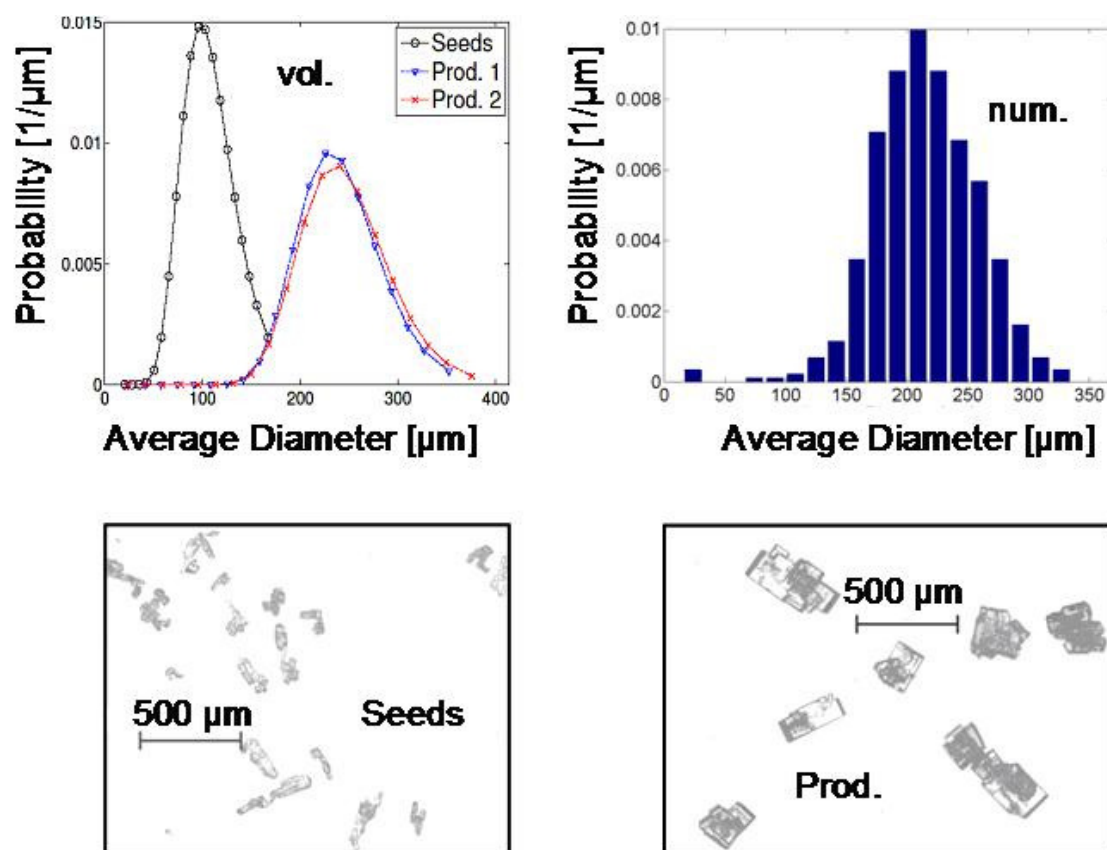


Figure 6-2: Crystallization with an ASA-EtOH solution flow of 13.4 mL/min (PI) and 3.8 mL/min of the seed suspension (PII). Top left corner: volume-density distributions of the seeds and two product samples. Top right corner: number density distribution of product (sample 2). Bottom: photos of seed and product crystals. Ref: Eder et al., *Crystal Growth & Design*, 2010

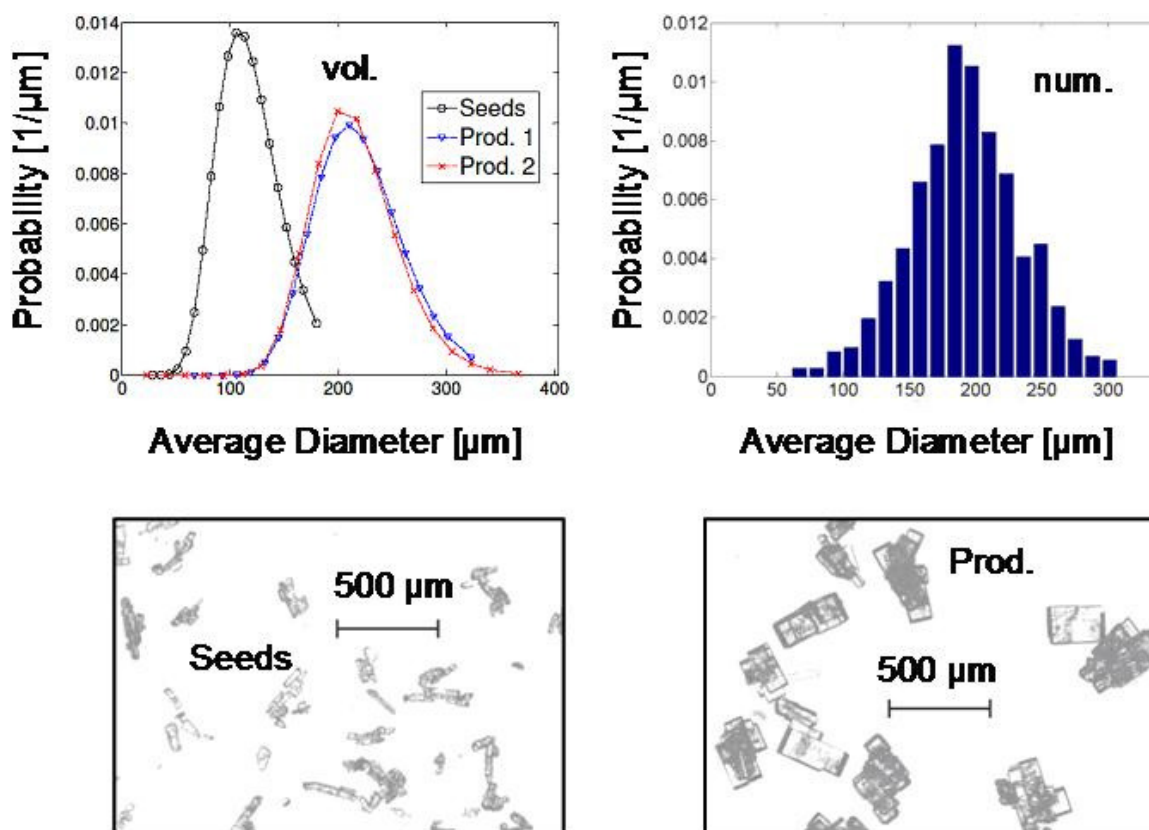


Figure 6-3: Crystallization with an ASA-EtOH solution flow of 17.8 mL/min (PI) and 5.0 mL/min of the seed suspension (PII). Top left corner: volume-density distributions of the seeds and two product samples. Top right corner: number density distribution of product (sample 2). Bottom: photos of seed and product crystals. *Ref.* Eder et al., *Crystal Growth & Design*, 2010

Figure 6-4, for a total flow of 25.2 mL/min, also shows good particle growth. The microscope pictures provide evidence of well shaped crystals and fewer agglomerates than with lower flow rates.

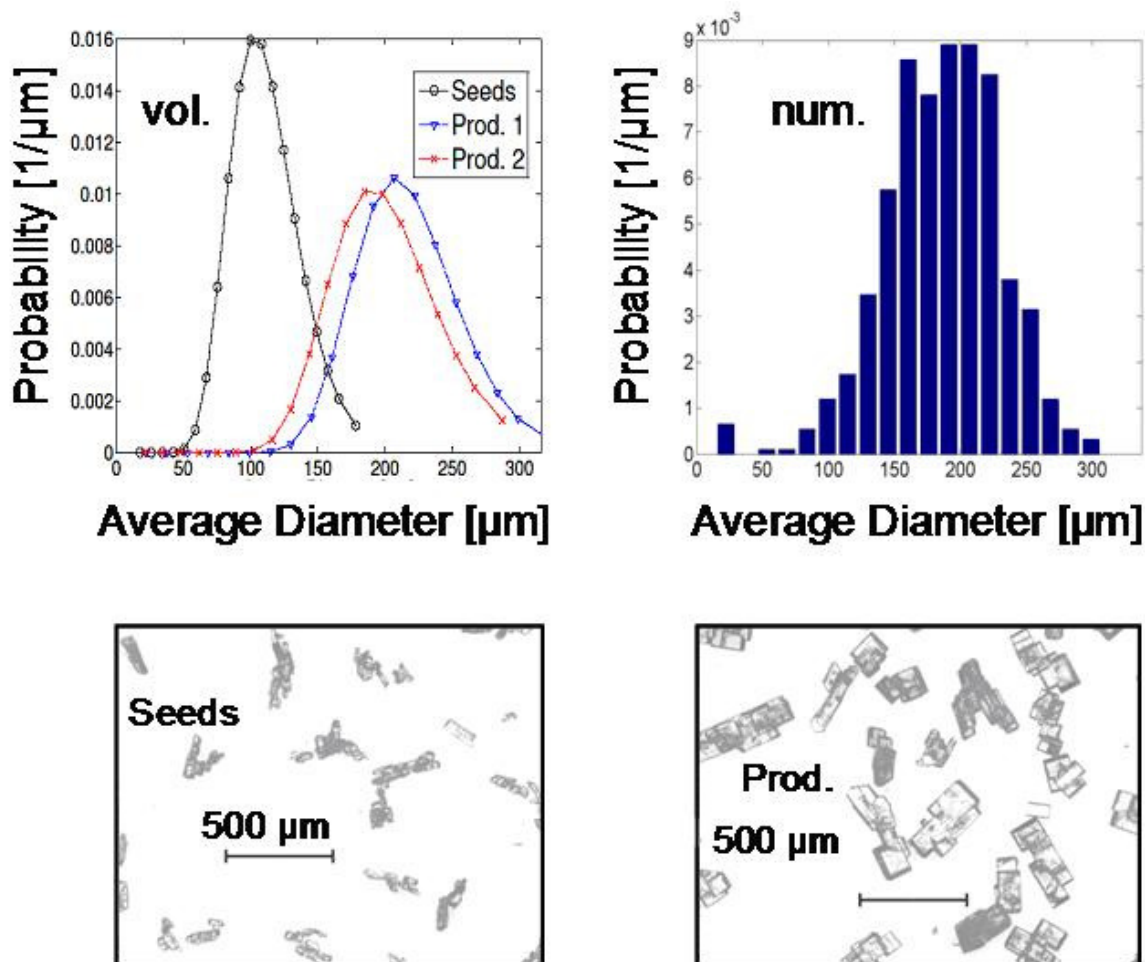


Figure 6-4: Crystallization with an ASA-EtOH solution flow of 19.7 mL/min (PI) and 5.5 mL/min of the seed suspension (PII). Top left corner: volume-density distributions of the seeds and two product samples. Top right corner: number density distribution of product (sample 2). Bottom: photos of seed and product crystals.

Overall it can be said that for all flow rates crystals growth was detected. The obtained particles were well-shaped and show slightly elongated cuboid structure. Agglomeration and crystal intergrowth diminish with increasing flow rates. In addition, steady state conditions were reached after little time. The single experiments (including taking two product samples) were done within only 15 minutes.

Table 6-1 summarizes the results obtained for the different flow experiments. It shows the flow rates of pump I and II (PI, PII), the time when samples were taken (t_{sample}), the mass gain during crystallization (m_{ASA}), the number and volume mean

diameters of seeds and products ($\bar{d}_{p,nmd}$, $\bar{d}_{p,vol}$) and their standard deviations (σ_{nmd} , σ_{vol}).

Table 6-1: Results for varying flow rates in a 15 m long tubular crystallizer.

Sample	PI [mL/min]	PII [mL/min]	t_{sample} [min]	m_{ASA} [g/min]	$\bar{d}_{p,nmd}$ [μ m]	σ_{nmd} [μ m]	$\bar{d}_{p,vol}$ [μ m]	σ_{vol} [-]
1-1 _{Seeds}	-	2.5	-	0.26	90	38	125	0.29
1-2 _{Product 1}	8.9	2.5	9	1.48	233	62	274	0.15
1-3 _{Product 2}	8.9	2.5	15	1.48	243	65	284	0.17
2-1 _{Seeds}	-	3.8	-	0.44	81	26	106	0.26
2-2 _{Product 1}	13.4	3.8	7	2.51	215	43	238	0.18
2-3 _{Product 2}	13.4	3.8	11	2.53	214	50	244	0.18
3-1 _{Seeds}	-	5.0	-	0.54	91	27	116	0.26
3-2 _{Product 1}	17.9	5.0	6	3.33	192	41	217	0.19
3-3 _{Product 2}	17.9	5.0	9	3.11	183	49	212	0.18
4-1 _{Seeds}	-	5.5	-	0.63	85	29	109	0.23
4-2 _{Product 1}	19.7	5.5	5	3.44	186	44	215	0.18
4-3 _{Product 2}	19.7	5.5	9	3.07	166	45	198	0.20

For determining the volume mean diameters $\bar{d}_{p,vol}$ mentioned in Table 6-1, the following logarithmic normal fitting function, Equation 32, has been used.

$$f(d_{p,vol}) = \frac{1}{\sigma_{vol} d_{p,vol} \sqrt{2\pi}} \exp \left[-\frac{1}{2} \left(\frac{\ln \left(\frac{d_{p,vol}}{\bar{d}_{p,vol}} \right)}{\sigma_{vol}} \right)^2 \right] \quad \text{Equation 32}$$

The number mean diameter $\bar{d}_{p,nmd}$ has been deduced directly from the microscope pictures. Equation 33 is based on the circle equivalent diameter (CED) of the i^{th} particle ($d_{p,i}$) and the total number of particles (N).

$$\bar{d}_{p,nmd} = \frac{1}{N} \sum_{i=1}^n d_{p,i} \quad \text{Equation 33}$$

The following table Table 6-2 lists up residence times (t_{res}), Reynolds numbers (Re), the mass of ASA per mL seed-suspension, mass gains (r_m , $r_{m,theor}$), the volume mean diameters of the experiments ($\bar{d}_{p,vol}$) and the ones calculated ($d_{p,calc}$) as well as the temperatures at the Y-branch feeding (T_{feed}) and at the end of the crystallizer (T_{prod}). For the calculation of the volume mean diameters MATLAB has been used.

Table 6-2: Residence times (t_{res}), Re-Numbers, mass of solid ASA per mL seed-suspension, mass gain (r_m) and the theoretical mass gain ($r_{m,theor}$) of the product to seed crystal masses, temperatures in the Y-fitting (T_{feed}) and the product temperature (T_{prod}) as well as the volume mean diameter ($\bar{d}_{p,vol}$) of the experiment and the calculated crystal diameter ($d_{p,calc}$) and their difference

flow rate [mL/min]	t_{res} [s]	Re [-]	$m_{seed}/mL_{seed-susp}$ [g/mL]	$r_{m,theor}$ [%]	r_m [%]	T_{feed} [°C]	T_{prod} [°C]	$\bar{d}_{p,vol}$ [μm]	$d_{p,calc}$ [μm]	$\Delta d_{p,calc}$ [μm]
11.4	248	10.8	0.10	655	569	34.4	24.6	279	189	90
17.2	164	16.3	0.11	617	588	39.7	24.2	241	189	52
22.8	124	21.7	0.11	615	595	39.9	25.3	215	185	30
25.2	112	24.0	0.11	562	517	40.5	26.3	207	184	23

The Reynolds numbers (Re) are all lower than the critical Reynolds number ($Re_{crit} \approx 2000$) and hence reveal a laminar flow regime. It is defined as

$$Re = \frac{\rho_{susp} \cdot v \cdot d_{inner}}{\mu} \quad \text{Equation 34}$$

The density of the suspension (ρ_{susp}) is 898 kg/m^3 at 40 °C and the inner diameter of the tubing (d_{inner}) is 0.002 m . The mean velocities of the suspension (v) are, according to the flow rates of Table 6-2, 0.06 , 0.09 , 0.12 and 0.13 m/s . The dynamic viscosity ($\mu = 0.01 \text{ Pa s}$) of the suspension has been measured with a rheometer at 25 °C (Physica - Anton Paar, MCR 300).

The constant mass values for solid ASA per mL seed-suspension at higher flow rates show a consistent extraction of seeds.

Furthermore, the actual mass gains have been calculated from the experimental results according to Equation 35. For the product mass the arithmetic mean mass flow (\dot{m}_{prod} [g/min]) has been used. The theoretical mass gain, however, is based on the Nývlt equation concentrations (see Equation 5) for the feed and product

temperatures, respectively. Therefore equilibrium conditions must be presumed. Equation 36 shows the calculation. The results are the increase of mass in percent.

$$r_m = \frac{\dot{m}_{prod}}{\dot{m}_{seeds}} \cdot 100 \quad \text{Equation 35}$$

$$r_{m,theor} = \frac{\Delta\dot{m}_{sol,theor} + \dot{m}_{seed} + \Delta\dot{m}_{seed,theor}}{\dot{m}_{seed}} \cdot 100 \quad \text{Equation 36}$$

As shown in Table 6-2 the actual mass gain was between 500 and 600%. This is still close to the theoretical achieved values. At the lowest flow rate (11.4 mL/min) the difference is a little higher. It can be assumed that due to the minor flow, the supersaturated solution already crystallizes in the Y-mixer. Thus the Y-branch gets partly plugged up and less material can pass. This decreases the product mass and hence the r_m value.

The differences between r_m and $r_{m,theor}$ for flow rates of 17.2 and 22.8 mL/min are almost constant. For 25.2 mL/min, however, there is a more significant difference. The foremost reason is expected to be the equilibrium. Due to the higher flow rate the residence time decreases and equilibrium cannot be reached. It means that at the end of the crystallizer the suspension is still slightly supersaturated. That contradicts the assumption made for the theoretical mass gain and leads to the deviation of the values.

In addition the volume mean diameters ($\bar{d}_{p,vol}$) of the achieved product crystals and the calculated volume mean diameters ($d_{p,calc}$), according to the simulation model, are compared. It can be seen that the experimental results are always above the calculations. This can be explained by the fact that the simulation neglects agglomeration (see chapter 5). Besides crystal growth also agglomeration is responsible for the size increase in the crystallizer, as was shown in the microscope pictures above. However, agglomeration decreases with higher flow rates and increased shear. Therefore, the results for a flow of 25.2 mL/min are quite good.

All experiments show a significant crystal growth. Figure 6-5 points out an inversely proportional relationship between growth and flow rate, which means crystals grow in direct proportion to the residence time in the crystallizer.

In the figure below three sets of experiments are displayed. For the graphs and microscope pictures (Figure 6-1, Figure 6-2, Figure 6-3, Figure 6-4) shown above and Table 6-1 only data of four different flows were chosen of a representative set of experiments. This was sufficient due to analog results.

The average diameter increases, $\Delta d_{p,vol}$ (the difference between seed diameters and the mean product diameters), are plotted as a function of their flow rates. Based on the figure a linear function can be assumed. This is more likely to be accidental than a fact.

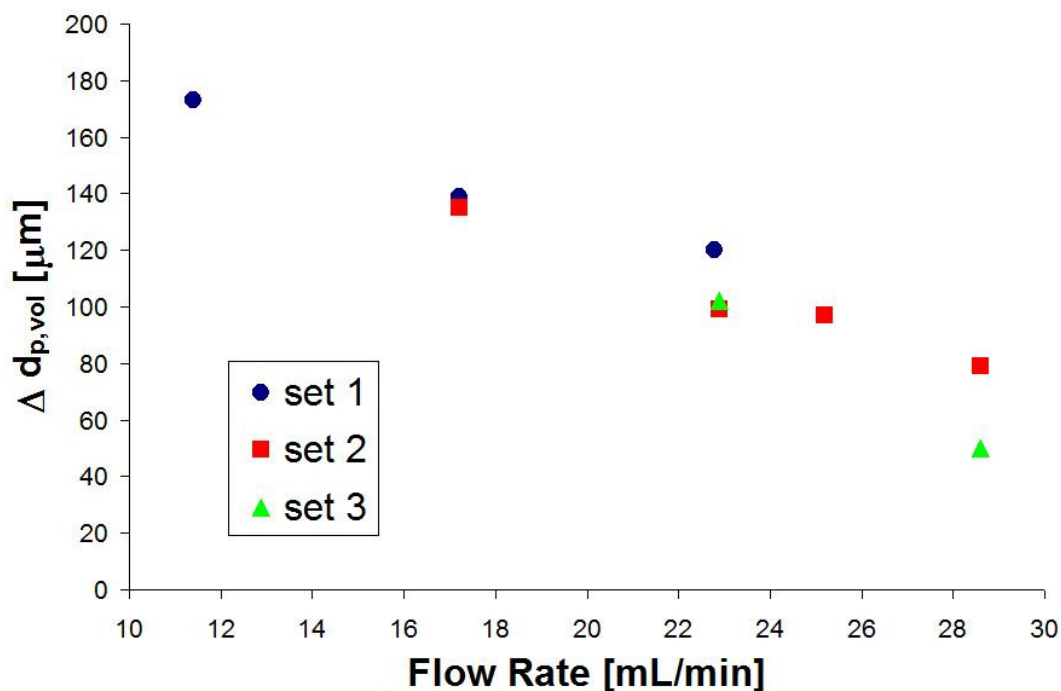


Figure 6-5: The average increase of the volume mean diameter from seed to product crystals as a function of flow rate. The mean value of two product samples has been used. Note that the dots, squares and triangles are based on data from different sets of experiments.

Nevertheless the inversely proportional trend was expected. Due to shorter residence times and higher end temperatures with increasing flow rates the decreasing growth can be explained. In addition, also less agglomeration happens with higher flows.

6.2. Temperature and Supersaturation Profiles

Temperature and supersaturation profiles were investigated and are shown for a flow of 17.2 mL/min representatively for all flows.

Simulation of Crystallization via Air Cooling

In Figure 6-6 the ASA solubility at equilibrium according to the Nývlt equation and the MATLAB calculated concentration over the length of the crystallizer are plotted. It shows that rapid cooling overbalances the system and equilibrium cannot be reached right away again. The generated supersaturation (see Equation 1) yields the crystal growth.

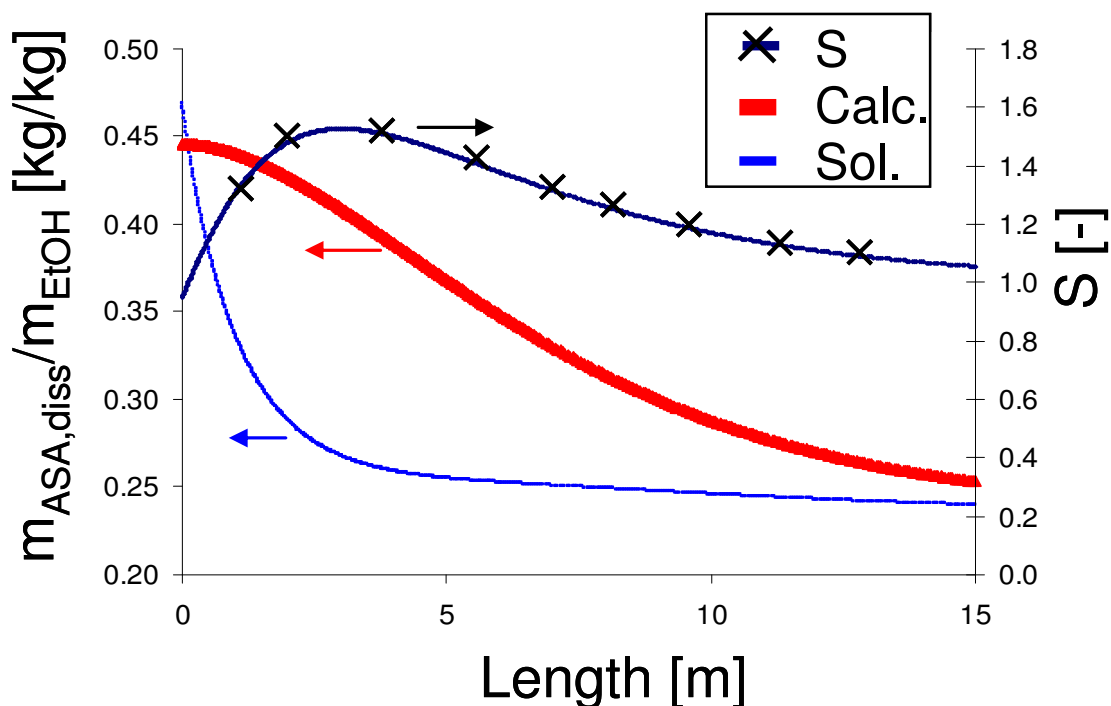


Figure 6-6: ASA solubility determined with Nývlt (Sol.), dissolved ASA computed according to the model presented in chapter 5 (Calc.) and the resulting supersaturation ratio (S) vs length. *Ref:* Eder et al., *Crystal Growth & Design*, 2010

The influence of the heat of crystallization on the temperature profile of the tubing is illustrated in Figure 6-7. It can be seen that there is no significant deviation. In both cases ambient temperature (T_{amb}) is almost achieved at the end. Moreover, a rapid temperature drop is discovered. The final temperature is almost reached after 5 m. The fast heat transfer can be ascribed to the small diameter of the tubing.

Additionally the increase in particle size along the crystallizer is shown.

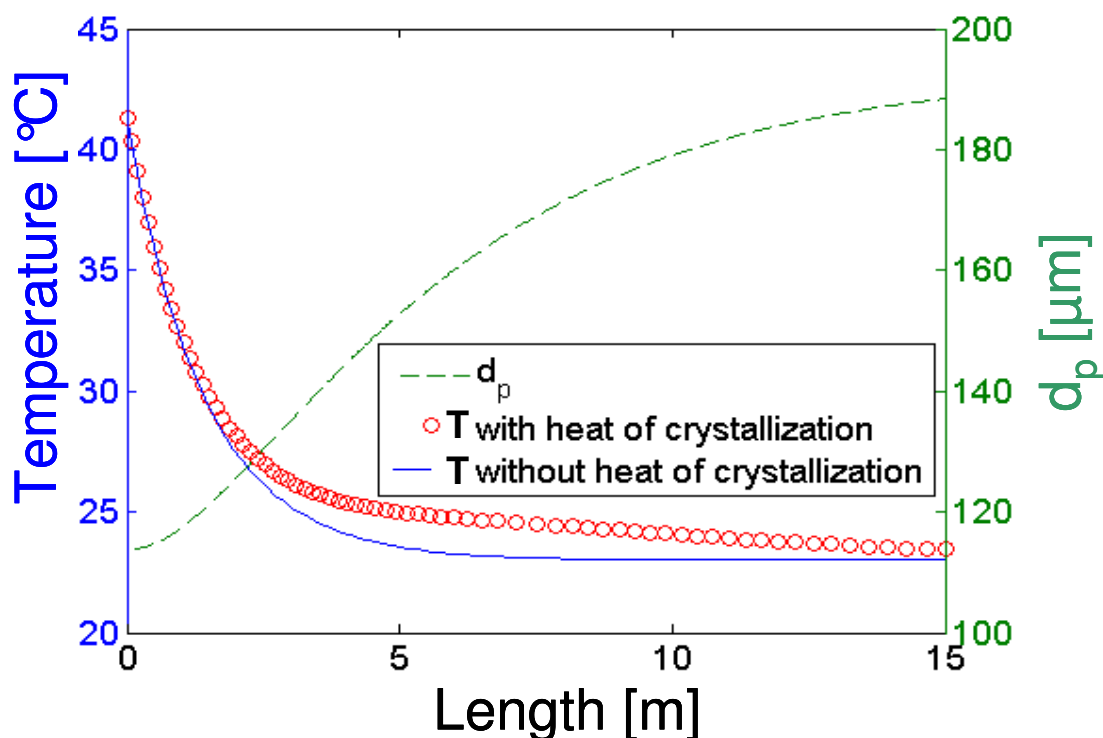


Figure 6-7: Temperature (T) with and without heat of crystallization and the increase of the particle diameter (d_p) versus the length of the crystallizer (flow rate = 22.8 mL/min). *Ref:* Eder et al., *Crystal Growth & Design*, 2010

The growth of the particles is also shown in Figure 6-8 for different flow rates. All results are based on a typical overall mass transfer coefficient of $K_g = 1.0 \cdot 10^{-5}$ m/s and the arithmetic mean of the volume mean diameters of the seeds of all experiments (i.e., $d_{av,seeds} = 114 \mu\text{m}$).

The sharp increase of size at the beginning is due to the rapid cooling and the resulting high supersaturation. As shown in Figure 6-6, the supersaturation rises at the beginning and exceeds a maximum. As it declines, also the slope of the particle size curve decreases. For a flow rate of 11.4 mL/min the growth slows down after 4.5 m. The growth rate for 17.2 mL/min decreases after the suspension has passed about 7 meters of the tubing and for the flows of 22.8 and 25.2 mL/min after about 8 – 9 m. All flows get close to equilibrium conditions and reach very similar product sizes.

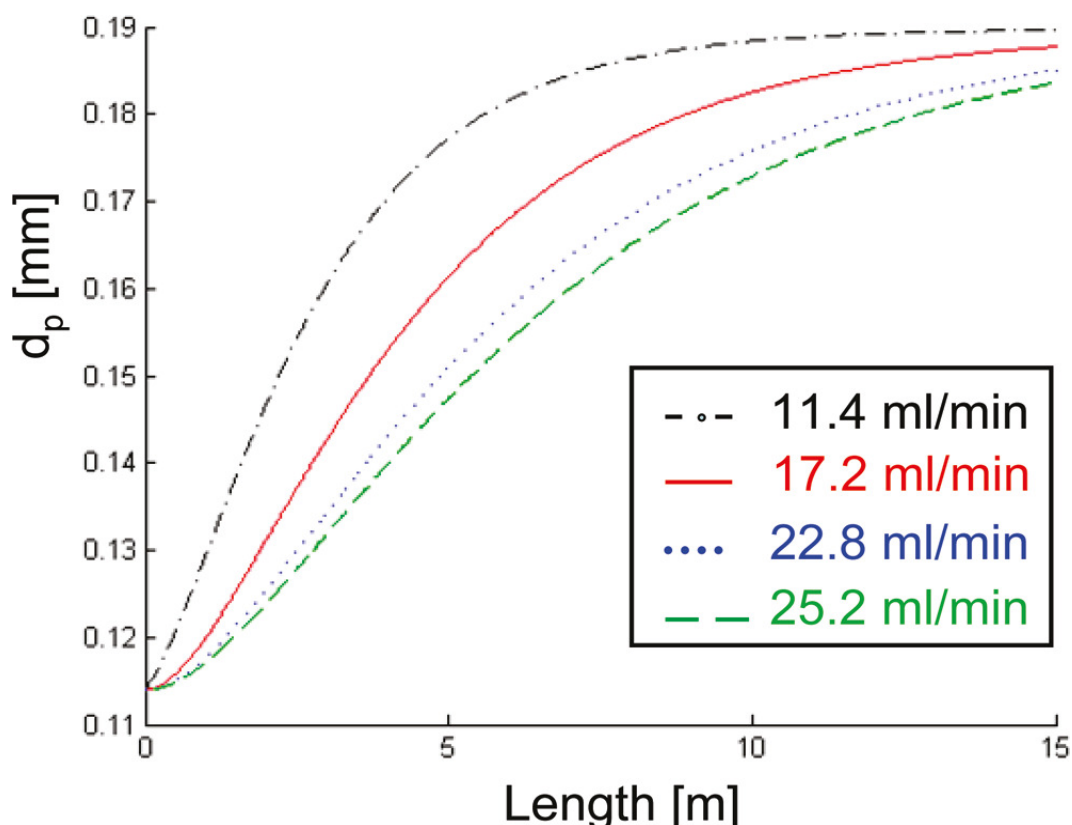


Figure 6-8: Growth of particles vs crystallizer length. An average of the mean seed diameters was used. Lines show the modeled increase of d_p . Ref: Eder et al., *Crystal Growth & Design*, 2010

Investigating an Optimized Temperature Profile

First an empirical study was conducted. Table 6-3 shows the temperatures and lengths selected for the particular water baths. The data refers to Figure 4-4.

Table 6-3: Experiments to find optimized temperature profiles. The data refers to the apparatus shown in Figure 4-4.

trial no.	T ₁ [°C]	L ₁ [m]	T ₂ [°C]	L ₂ [m]	T ₃ [°C]	L ₃ [m]	comment
1	32	8	26	7	-	-	
2	32	5	23	10	-	-	pipe plugs in bath 2
3	32	5	26	3	22	7	pipe plugs in bath 2
4	32	5	27	3	22	7	

The temperature drop between the first and second bath in experiment two and three has been too sudden. The supersaturation gets too high which results in primary nucleation and pipe plugging in the second bath.

Figure 6-9 shows the MATLAB simulation of trial number 1 and 2 in comparison. While trial 1 has worked perfectly trial 2 has a too rapid temperature change.

Hence the supersaturation rises too expeditiously at the beginning of the second bath. The result is the plugging of the tubing in bath 2.

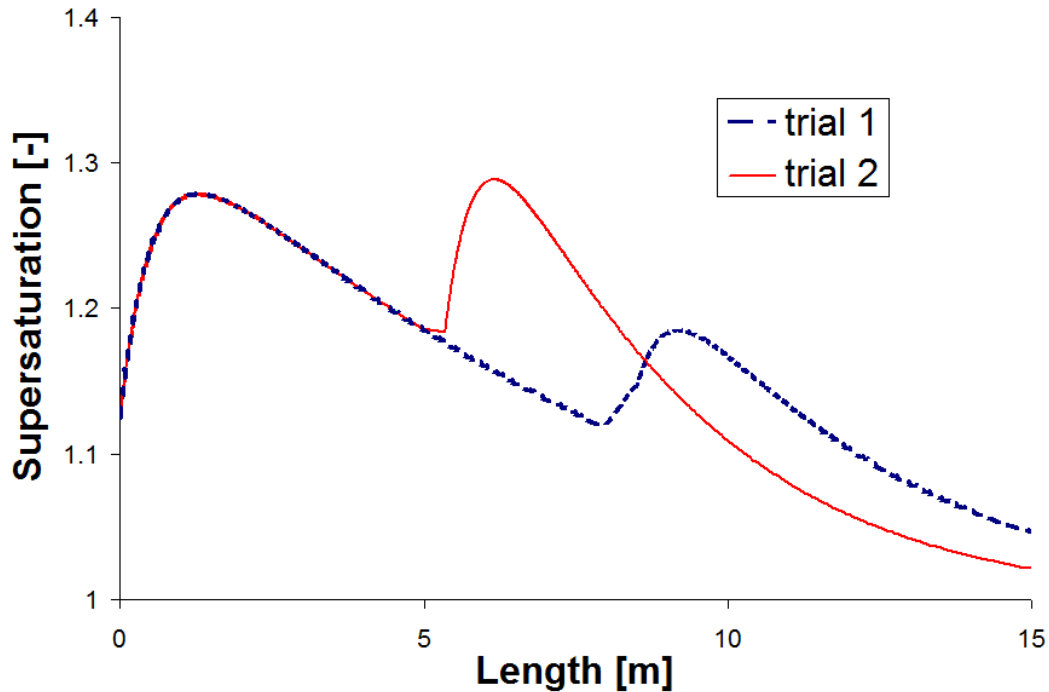


Figure 6-9: Supersaturation profile for trial number 1 (1st bath: 8 m, 32 °C; 2nd bath: 7 m, 26 °C) and trial number 2 (1st bath: 5 m, 32 °C; 2nd bath: 10 m, 23 °C). In trial 2 the temperature change was too sudden, supersaturation rose too fast at the beginning of the second bath and caused pipe plugging.

In order to receive a more affective temperature trajectory, a third water bath was attached for trial 3 and 4. The achieved supersaturation profile for trial 4 is demonstrated in Figure 6-10 in comparison with the original one from the variation of flow experiments.

Supersaturation is going to more constant values with the use of different cooling steps. The obtained crystals have a better shape and the building of fines is prevented. In addition the risk of plugging is reduced too.

In the end equilibrium conditions are approached by both experiments.

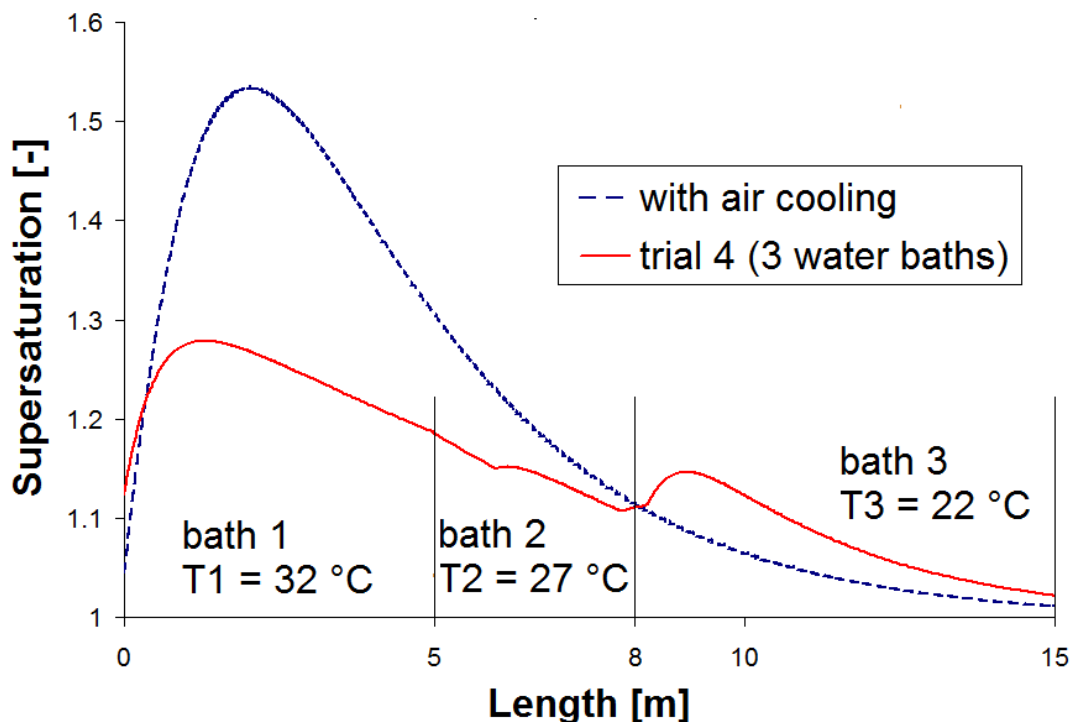


Figure 6-10: Supersaturation profile for experiments with air cooling and for trial 4, cooling with 3 water baths.

The results concerning the investigation of an optimized temperature profile are based on preliminary tests. The goal of reaching a more constant supersaturation profile (see Figure 4-3) has been approached. Further investigations are necessary to obtain an optimal temperature trajectory and thus perfect growing conditions for crystals. Continuative studies include the use of additional water cooling baths or the implementation of counter- and cross current cooling flows.

6.3. Variation of Seed Loading

The influence in crystal size distribution of four different seed loadings was investigated. One experiment for each loading was chosen for detailed studies.

As shown in Figure 6-11 a shift in particle size from seeds to product crystals is obvious for all amounts of seed loadings. Also a trend from larger to smaller volume mean diameters with increasing seed loading can be discovered.

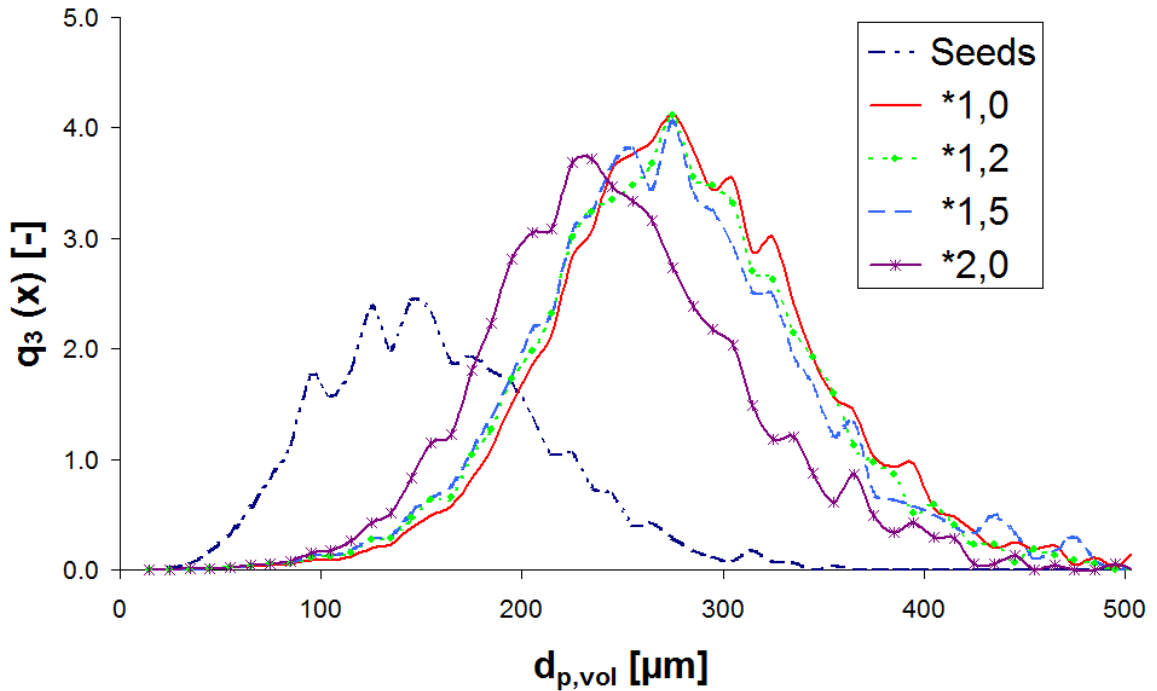


Figure 6-11: q_3 distributions of an average seed sample and of product crystals gained by trials with different seed loadings.

Although these shifts are rather small, Figure 6-12 shows that there definitely is an interdependence between loading and product size detectable. The average diameter increases, $\Delta d_{p,vol}$ (the difference between the mean seed diameters and the mean product diameters), are plotted against the seed loadings (mass of solids per mL seed suspension). A higher loading results in a larger number of smaller product crystals. While having a low seed loading gives less but bigger product particles. The same amount of surplus ASA from the supersaturated suspension grows on a different number of seeds. This leads to the shown inversely proportional relationship.

From Figure 6-12 a clear trend can be seen.

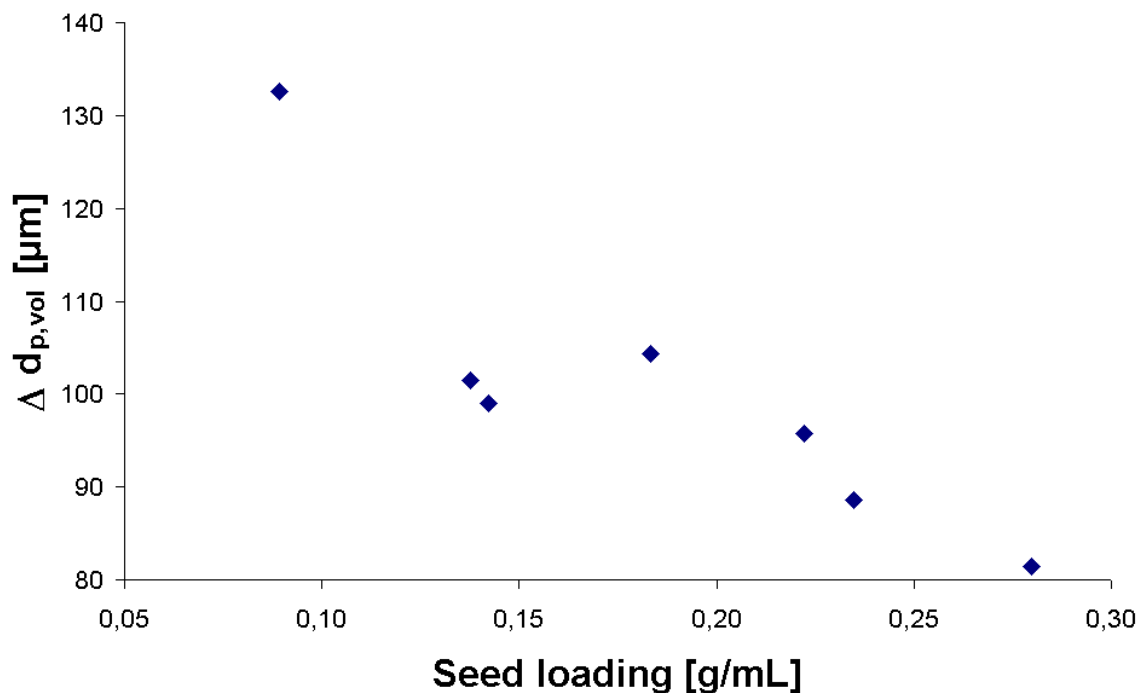


Figure 6-12: The average increase in diameter during the crystallization as a function of seed loading. The mean values of two seed samples and two product samples have been used, respectively.

With higher seed loading also the possibility of agglomeration increases.

Figure 6-13 illustrates seeds and product crystals for different initial loadings. The bottom right picture that refers to a double seed loading, shows a number of small crystals that form agglomerates, whereas the bottom left crystals for *1.2 loading are larger and less agglomerated. An upper limit for seed loading can be assumed in order to keep agglomeration low.

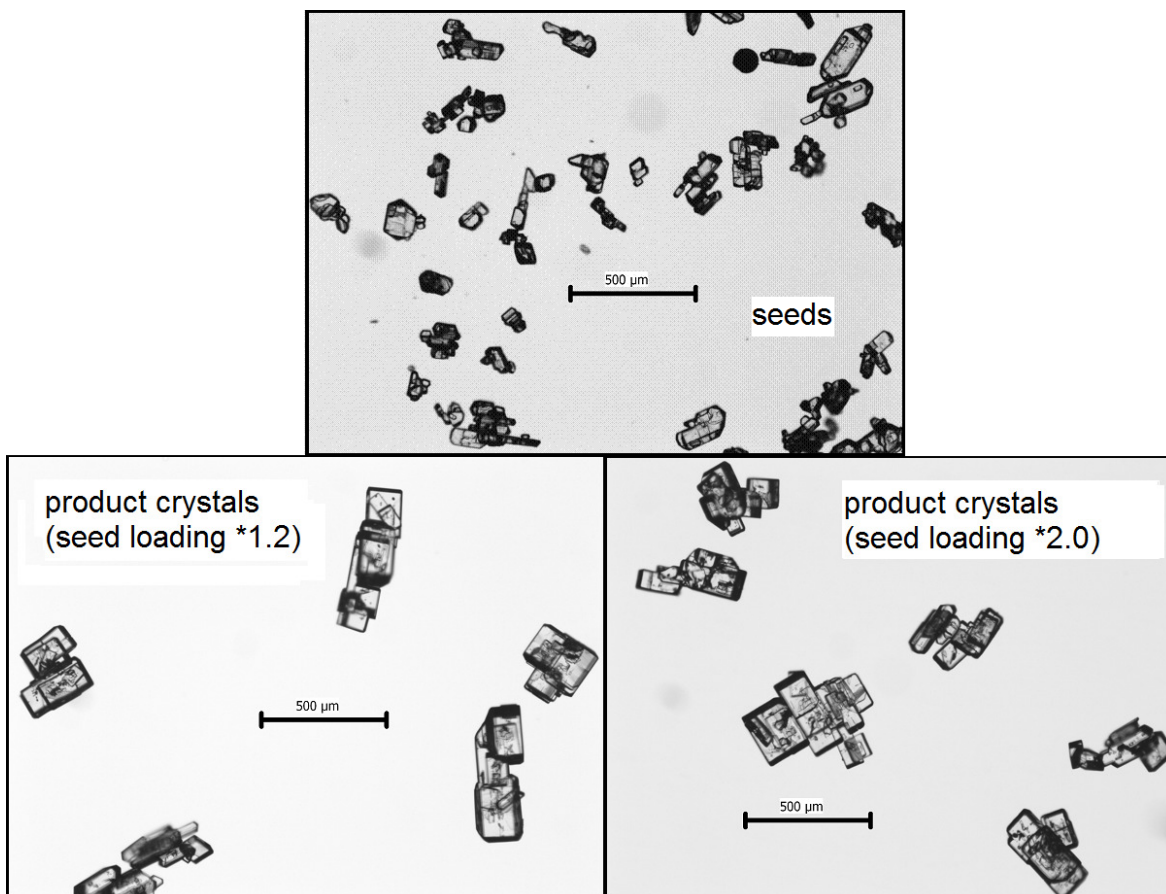


Figure 6-13: Seeds and product crystals for different seed loadings. Top: Seed crystals. Left: product crystals for a loading of *1.2. Right: product crystals for a loading of *2.0.

Table 6-4 sums up the results obtained for the experiments with different seed loadings. The mass of seeds per mL seed suspension gives the actual loading. It is achieved through the output weight of the particular seeds samples and the flow rate. The flow rates have been kept constant. Moreover, the mass gains during crystallization and the volume mean diameters are shown.

Table 6-4: Results for different seed loadings

Sample	Calc. seed loading factor [-]	$m_{\text{seed}}/mL_{\text{seed-susp}}$ [g/mL]	PI [mL/min]	PII [mL/min]	t_{sample} [min]	m_{ASA} [g/min]	$d_{p,\text{vol}}$ [μm]
1-1 _{Seeds 1}			-	3,8	-	0,3246	119,66
1-2 _{Product 1}	*1	0,09	13,1	3,8	5	2,7342	257,42
1-3 _{Product 2}			13,1	3,8	8	2,7212	263,08
1-4 _{Seeds 2}			-	3,8	-	0,3538	127,87
2-1 _{Seeds 1}			-	3,8	-	0,6385	152,59
2-2 _{Product 1}	*1.2	0,14	13,1	3,8	8	2,7550	256,12
2-3 _{Product 2}			13,1	3,8	13	2,7516	257,43
2-4 _{Seeds 2}			-	3,8	-	0,4072	149,43
3-1 _{Seeds 1}			-	3,8	-	0,7501	145,56
3-2 _{Product 1}	*1.5	0,18	13,1	3,8	8	2,8580	253,36
3-3 _{Product 2}			13,1	3,8	11	2,8410	256,73
3-4 _{Seeds 2}			-	3,8	-	0,6434	144,73
4-1 _{Seeds 1}			-	3,8	-	0,9158	125,06
4-2 _{Product 1}	*2.0	0,22	13,1	3,8	4	2,9014	227,65
4-3 _{Product 2}			13,1	3,8	11	2,9422	225,56
4-4 _{Seeds 2}			-	3,8	-	0,7734	127,82

6.4. QICPIC vs. Microscope Analysis

To compare the two selected analysis methods, QICPIC and microscope, Figure 6-14 has been plotted. Although the microscope data is based on a far smaller number of crystals viewed, it definitely gives the same trends as the QICPIC analysis.

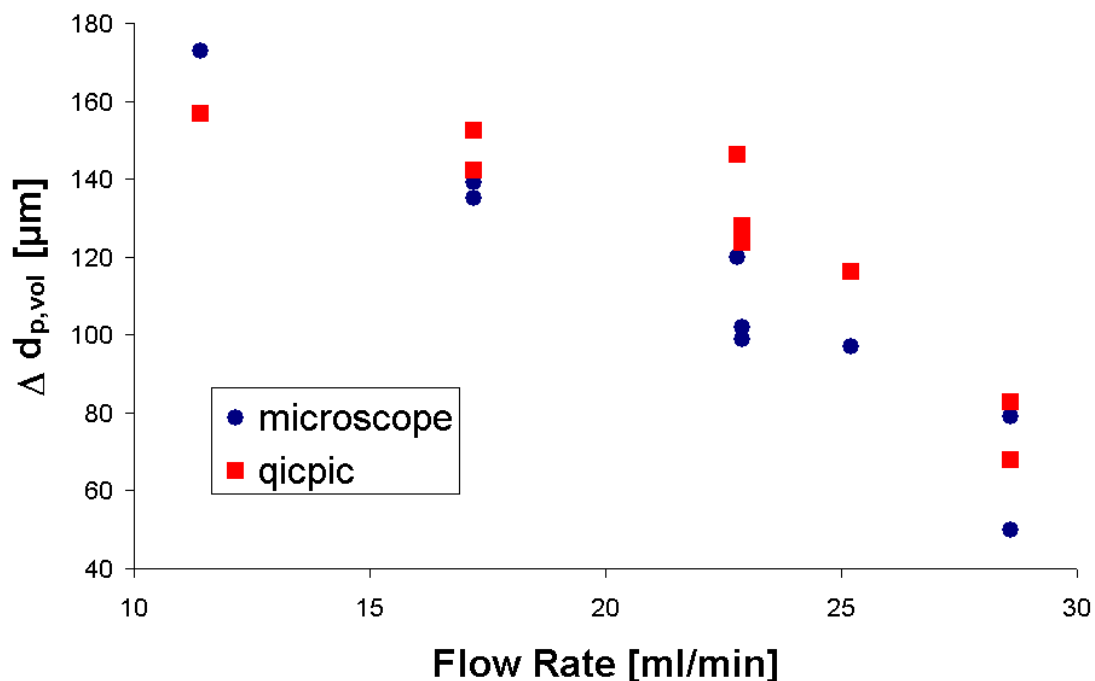


Figure 6-14: Comparison of microscope analysis and QICPIC analysis for the flow rate experiments

Generally speaking using QICPIC comes with a number of advantages. While determining CSDs for just a single sample took up to two hours with the microscope, QICPIC just took a view seconds once all parameters had been set. In addition a far larger amount of crystals can be viewed and data can be compared much easier. The microscope, however, is certainly the cheaper and usually better available method. Therefore Figure 6-14 proves that it is a legitimate analysis method for the given crystal samples.

7. Conclusion

A novel, versatile, continuously seeded, continuously operated tubular crystallizer system (CSCOTC) has been developed and tested for the crystallization of active pharmaceutical ingredients (APIs) under controlled conditions. The continuously working crystallizer allows the independent control of single process parameters. In a first set of experiments flow rates (and thus the residence times) were varied while in the second set the influence of seed loading was investigated. Therefore a tube with a length of 15 m and an inner diameter of 2.0 mm was used. It was fed with a seed suspension stream and a slightly undersaturated solution that was kept at an elevated temperature in its storage vessel. Supersaturation was created via cooling. Acetylsalicylic acid (ASA) was crystallized as a model substance from ethanol (EtOH).

The aim of this work was the proof of concept and the study of influences such as flow rates and seed loadings.

For the first set of experiments flow rates were varied between 11.4 mL/min and 28.6 mL/min. The main results are:

- The concept of the CSCOTC has been proven feasible. Effects such as pipe plugging can easily be controlled by variation of settings. Only for seed feed flow rates of 2.5 mL/min the crystallizer got plugged. This was due to nucleation that occurred because no seeds were present in the crystallizer.
- Experiments for all feed flows showed detectable increases in mean particle diameters and a shift of the volume density distribution towards larger values. Comparing the results from the experiments with the simulation reveals particle size differences due to agglomeration effect. Agglomeration decreases with increasing flow rate. In this work agglomeration has been neglected for all calculations.
- An inversely proportional relationship between growth and flow rate was established, which means growth is in direct proportion to the residence time.

- The obtained product crystals were well-shaped and showed slightly elongated cuboid structure.
- Equilibrium conditions in the crystallizer were reached immediately as crystal size distributions (CSDs) and masses of the two product samples in every experiment showed.
- Scale up can easily be implemented by numbering up.

The main results for the variation of seed loading experiments are the followings:

- All experiments showed significant increases in mean particle diameters and a shift of the volume density distribution towards larger values.
- The mean particle size of the product crystals decreased with increasing seed loading.
- Higher seed loadings increasingly led to agglomeration.

In summary, the objects of this work were achieved. A feasible continuously seeded, continuously operated tubular crystallizer was developed and successfully operated. Variation of different process parameters led to the expected variation in product crystal sizes.

8. Outlook

The continuously seeded, continuously operated tubular crystallizer is now tested with other model substances, such as paracetamol and ibuprofen. First successes have already been registered.

Moreover, in this work seeds were produced batch wise. The aim of further studies should be the continuous seed production. Therefore, the implementation of a recycling stream that recycles, mills and classifies a fraction of the product stream, to use it as the seed inlet into the crystallizer, is one of the future goals of this project.

Other future prospects are coating of particles and polymorphism control in the continuously seeded, continuously operated tubular crystallizer.

9. Appendix

9.1. Preparation of Seeds with ASA from GL Pharma

Due to a large PSD and far too large particles in the GL Pharma ASA (see Figure 9-1) a preparation step became necessary. The goal was to get smaller and more constant seeds than those achieved by agitation only.

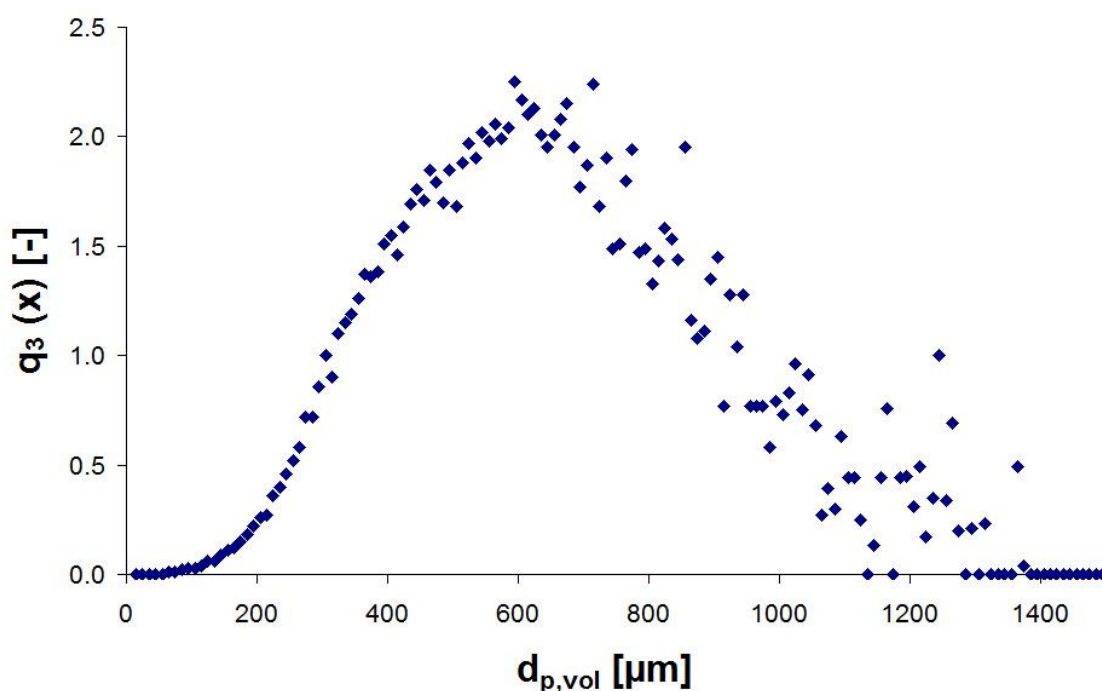


Figure 9-1: q_3 distribution of ASA raw material from GL Pharma

The desired amount of ASA and EtOH was weighed out into a one liter glass vessel. It was dissolved in a 62 °C water bath under continuous stirring. To precipitate ASA a cooling bath (ice and water) and ultrasound was used. Moreover, a constant agitation at high speed was necessary. After four minutes of precipitation on ice the suspension was put into a room temperature water bath. It was kept stirring under ultrasound for another hour. Then ultrasound was turned off and the suspension was kept stirring at room temperature over night to reach equilibrium.

The achieved particle size distribution is shown in Figure 9-2. Although different amounts of ASA were weighed out and prepared for experimentation, their

distribution is still the same. The mean particle size is now between 130-160 μm and the standard deviation diminishes significantly as well.

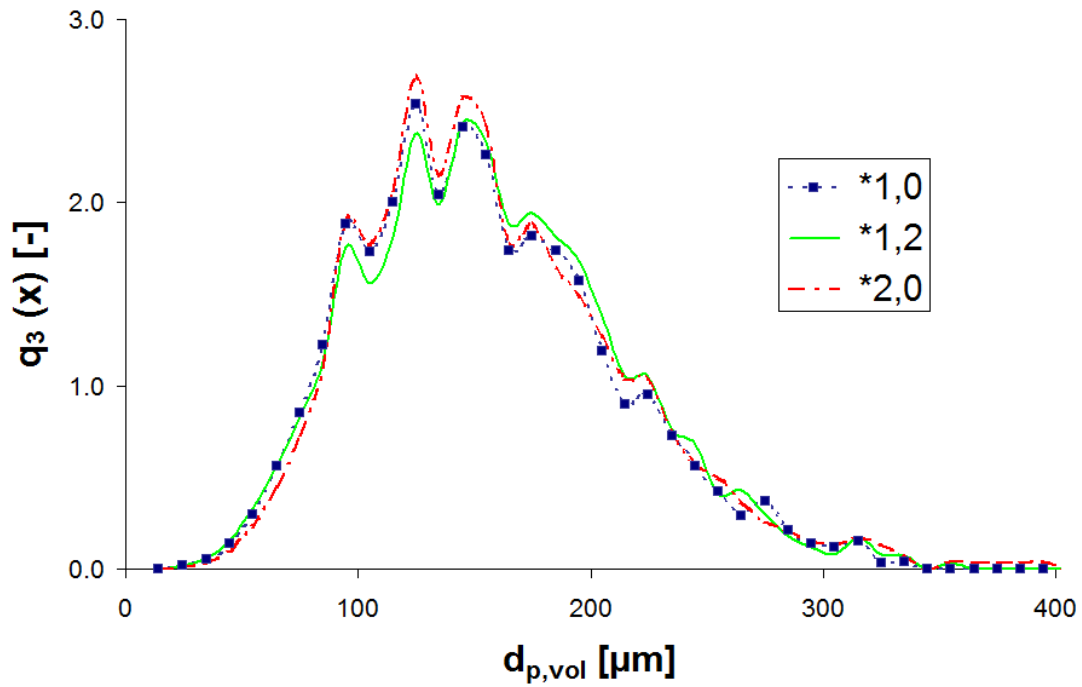


Figure 9-2: q_3 distributions of ASA from GL Pharma after the preparation. Seeds for different seed loading experiments get same particle size distribution.

9.2. QICPIC Settings

QICPIC (QP0112) & OASISDRY/L, 2.00 63.0 mm - M8 (20...6820µm)

Analysis: WINDOX 5.5.4.0

Product: ASA

Calculation base method: EQPC

Density: 1.3500 g/cm³

Class limits: M8

Optical Concentration: 0,14 %

Trigger conditions: "ASA"

User parameters:

Start: concentration \geq 0,01%

Validity: always

Stop: 5s optical Concentration \leq 0,01% or 999s real time

Reference List

- (1) Eder RJP, Radl S, Schmitt E, Innerhofer S, Maier M, Gruber-Woelfler H et al. Continuously Seeded, Continuously Operated Tubular Crystallizer for the Production of Active Pharmaceutical Ingredients. *Crystal Growth & Design*. 2010; 10:2247-2257.
- (2) Eder RJP, Gruber-Woelfler H, Khinast JG. Kontinuierliches Kristallisation in einem Rohrkristallisator. *Chemie Ingenieur Technik* 81[8], 1171. 2010.
- (3) Chen LA, Li J, Matsuoka M. Experimental and theoretical investigation of the purification process of organic materials in a continuous inclined column crystallizer. *Industrial & Engineering Chemistry Research*. 2006; 45:2818-2823.
- (4) Tavare NS, Matsuoka M, Garside J. Modelling a continuous column crystallizer: Dispersion and growth characteristics of a cooling section. *Journal of Crystal Growth*. 1990; 1151-1155.
- (5) Myerson AS. *Handbook of Industrial Crystallization*. 2nd ed ed. Boston Oxford Johannesburg Melbourne New Delhi Singapore: Butterworth-Heinemann, 2002.
- (6) Mullin JW. *Crystallization*. 3rd ed. Oxford Boston Johannesburg Melbourne New Delhi Singapore: Butterworth-Heinemann, 1992.
- (7) Lindenberg C, Krattli M, Cornel J, Mazzotti M, Brozio J. Design and Optimization of a Combined Cooling/Antisolvent Crystallization Process. *Crystal Growth & Design*. 2009; 9:1124-1136.
- (8) Barrett P, Smith B, Worlitschek J, Bracken V, O'Sullivan B, O'Grady D. A review of the use of process analytical technology for the understanding and optimization of production batch crystallization processes. *Organic Process Research & Development*. 2005; 9:348-355.
- (9) Hammond RB, Pencheva K, Ramachandran V, Roberts KJ. Application of grid-based molecular methods for modeling solvent-dependent crystal growth morphology: Aspirin crystallized from aqueous ethanolic solution. *Crystal Growth & Design*. 2007; 7:1571-1574.
- (10) Ulrich J. Solution crystallization - Developments and new trends. *Chemical Engineering & Technology*. 2003; 26:832-835.
- (11) Hofmann Guenter. *Kristallisation in der Industriellen Praxis*. Weinheim: Wiley-VCH, 2004.
- (12) Togkalidou T, Braatz RD, Johnson BK, Davidson O, Andrews A. Experimental design and inferential modeling in pharmaceutical crystallization. *Aiche Journal*. 2001; 47:160-168.

- (13) Alvarez Aj, Myerson AS. Continuous Plug Flow Crystallization of Pharmaceutical Compounds. *Crystal Growth & Design*. 2010; 10:2219-2228.
- (14) Doki N, Yokota M, Kido K, Sasaki S, Kubota N. Reliable and selective crystallization of the metastable alpha-form glycine by seeding. *Crystal Growth & Design*. 2004; 4:103-107.
- (15) Chow K, Tong HHY, Lum S, Chow AHL. Engineering of pharmaceutical materials: An industrial perspective. *Journal of Pharmaceutical Sciences*. 2008; 97:2855-2877.
- (16) Fujiwara M, Nagy ZK, Chew JW, Braatz RD. First-principles and direct design approaches for the control of pharmaceutical crystallization. *Journal of Process Control*. 2005; 15:493-504.
- (17) Sarkar D, Rohani S, Jutan A. Multi-objective optimization of seeded batch crystallization processes. *Chemical Engineering Science*. 2006; 61:5282-5295.
- (18) Oullion M, Puel F, Fevotte G, Righini S, Carvin P. Industrial batch crystallization of a plate-like organic product. In situ monitoring and 2D-CSD modelling. Part 2: Kinetic modelling and identification. *Chemical Engineering Science*. 2007; 62:833-845.
- (19) Oullion M, Puel F, Fevotte G, Righini S, Carvin P. Industrial batch crystallization of a plate-like organic product. In situ monitoring and 2D-CSD modelling: Part 1: Experimental study. *Chemical Engineering Science*. 2007; 62:820-832.
- (20) Winn D, Doherty MF. A new technique for predicting the shape of solution-grown organic crystals. *Aiche Journal*. 1998; 44:2501-2514.
- (21) Winn D, Doherty MF. Modeling crystal shapes of organic materials grown from solution. *Aiche Journal*. 2000; 46:1348-1367.
- (22) Shekunov BY, Chattopadhyay P, Tong HHY, Chow AHL. Particle size analysis in pharmaceuticals: Principles, methods and applications. *Pharmaceutical Research*. 2007; 24:203-227.
- (23) Gros H, Kilpio T, Nurmi J. Continuous cooling crystallization from solution. *Powder Technology*. 2001; 121:106-115.
- (24) Variankaval N, Cote AS, Doherty MF. From form to function: Crystallization of active pharmaceutical ingredients. *Aiche Journal*. 2008; 54:1682-1688.
- (25) Yu LX, Lionberger RA, Raw AS, D'Costa R, Wu HQ, Hussain AS. Applications of process analytical technology to crystallization processes. *Advanced Drug Delivery Reviews*. 2004; 56:349-369.
- (26) Birch M, Fussell SJ, Higginson PD, McDowall N, Marziano I. Towards a PAT-Based strategy for crystallization development. *Organic Process Research & Development*. 2005; 9:360-364.

- (27) Fevotte G. New perspectives for the on-line monitoring of pharmaceutical crystallization processes using in situ infrared spectroscopy. *International Journal of Pharmaceutics*. 2002; 241:263-278.
- (28) LaPorte TL, Wang C. Continuous processes for the production of pharmaceutical intermediates and active pharmaceutical ingredients. *Current Opinion in Drug Discovery & Development*. 2007; 10:738-745.
- (29) Midler MJr, Liu PD, Paul EL, Futran M, Whittington EF. A crystallization method to improve crystal structure and size. EP. 1991; 0461930A1.
- (30) Brenek SJ, AM Ende DJ. Crystallization method and apparatus using an impinging plate assembly. US Patent. 2004; 0040098839.
- (31) Dombrowski RD, Litster JD, Wagner NJ, He Y. Crystallization of alpha-lactose monohydrate in a drop-based microfluidic crystallizer. *Chemical Engineering Science*. 2007; 62:4802-4810.
- (32) Su YF, Kim H, Kovenklioglu S, Lee WY. Continuous nanoparticle production by microfluidic-based emulsion, mixing and crystallization. *Journal of Solid State Chemistry*. 2007; 180:2625-2629.
- (33) Myerson AS. Molecular crystals of controlled size. US Patent. 2003; 0030170999.
- (34) Gerdts CJ, Tereshko V, Yadav MK, Dementieva I, Collart F, Joachimiak A et al. Time-controlled microfluidic seeding in nL-volume droplets to separate nucleation and growth stages of protein crystallization. *Angewandte Chemie-International Edition*. 2006; 45:8156-8160.
- (35) Schiewe J, Zierenberg B. Process and apparatus for producing inhalable medicaments. US Patent. 2003; 2003/0015194A1.
- (36) Méndez del Rio JR, Rousseau RW. Batch and tubular-batch crystallization of paracetamol: Crystal size distribution and polymorph formation. *Crystal Growth & Design*. 2006; 6:1407-1414.
- (37) Tan H, Reed M, Gahm KH, King T, Seran MD, Bostick T et al. An integrated high-throughput screening approach for purification of solid organic compounds by trituration and crystallization in solvents. *Organic Process Research & Development*. 2008; 12:58-65.
- (38) Cui Y. A material science perspective of pharmaceutical solids. *International Journal of Pharmaceutics*. 2007; 339:3-18.
- (39) Beckmann W. Seeding the desired polymorph: Background, possibilities, limitations, and case studies. *Organic Process Research & Development*. 2000; 4:372-383.
- (40) Yu L, Reutzel SM, Stephenson GA. Physical characterization of polymorphic drugs: an integrated characterization strategy. *Pharmaceutical Science & Technology Today*. 1998; 1:118-127.

- (41) Wang F, Wachter JA, Antosz FJ, Berglund KA. An investigation of solvent mediated polymorphic transformation of progesterone using in situ Raman spectroscopy. *Organic Process Research & Development*. 2000; 4:391-395.
- (42) Zencirci N, Gelbrich T, Kahlenberg V, Griesser UJ. Crystallization of Metastable Polymorphs of Phenobarbital by Isomorphic Seeding. *Crystal Growth & Design*. 2009; 9:3444-3456.
- (43) Braun DE, Gelbrich T, Kahlenberg V, Tessadri R, Wieser J, Griesser UJ. Stability of Solvates and Packing Systematics of Nine Crystal Forms of the Antipsychotic Drug Aripiprazole. *Crystal Growth & Design*. 2009; 9:1054-1065.
- (44) Vishweshwar P, McMahon JA, Oliveira M, Peterson ML, Zaworotko MJ. The predictably elusive form II of aspirin. *Journal of the American Chemical Society*. 2005; 127:16802-16803.
- (45) Bond AD, Boese R, Desiraju GR. On the polymorphism of aspirin: Crystalline aspirin as intergrowths of two "polymorphic" domains". *Angewandte Chemie-International Edition*. 2007; 46:618-622.
- (46) Maia GD, Giulietti M. Solubility of acetylsalicylic acid in ethanol, acetone, propylene glycol, and 2-propanol. *Journal of Chemical and Engineering Data*. 2008; 53:256-258.
- (47) Kirklin DR. Enthalpy of combustion of acetylsalicylic acid. *Journal of Chemical Thermodynamics*. 2000; 32:701-709.
- (48) Bird RB, Stewart WE, Lightfoot EN. *Transport Phenomena*. 2 ed ed. John Wiley and Sons, Inc., 2002.
- (49) Granberg RA, Bloch DG, Rasmuson AC. Crystallization of paracetamol in acetone-water mixtures. *Journal of Crystal Growth*. 1999; 199:1287-1293.
- (50) Granberg RA, Rasmuson AC. Crystal growth rates of paracetamol in mixtures of water plus acetone plus toluene. *Aiche Journal*. 2005; 51:2441-2456.